

Flat spectra of cosmic gravitons in the nHz and audio bands

Massimo Giovannini ¹

Department of Physics, CERN, 1211 Geneva 23, Switzerland

INFN, Section of Milan-Bicocca, 20126 Milan, Italy

Abstract

The spectra of the relic gravitons are customarily normalized in the low-frequency domain where the signal of the concordance paradigm is expected to peak and this is why their contribution to the temperature and polarization anisotropies of the microwave background is only described by the tensor to scalar ratio. If the consistency relations are broken, the same strategy is accomplished by introducing the tensor spectral index as a further independent parameter. When the dominant component of the spectral energy density is distributed for frequencies much larger than the aHz, the logic behind this conventional approach is much less compelling. The improved bounds in the audio band and the current data from the pulsar timing arrays in the nHz region motivate a new strategy for the absolute normalization of the cosmic background of relic gravitons. After introducing a general four-dimensional action for the analysis of the relic gravitons the new approach is illustrated in the case of conventional and unconventional inflationary models.

¹Electronic address: massimo.giovannini@cern.ch

1 Introduction

Since the evolution of the tensor modes of the geometry is not Weyl-invariant [1, 2, 3] the production of relic gravitons is expected, with different phenomenological signatures, in a variety of scenarios and, in particular, during an isotropic phase of quasi-de Sitter expansion [4]. Besides the vanilla Λ CDM paradigm², the simplest version of the concordance scenario includes only one further free parameter, namely the ratio $r_T(k_p)$ describing the tensor component of the large-scale inhomogeneity at a conventional pivot scale (see e.g. [5, 6, 7]) that coincides, in what follows, with $k_p = 0.002 \text{ Mpc}^{-1}$. This scale corresponds³ to a comoving frequency $\nu_p = k_p/(2\pi) = 3.09 \text{ aHz}$ and this is why, in the conventional lore, the limits on $r_T(k_p)$ translate into constraints on the spectral energy density of the relic gravitons in the aHz range. The spectral energy density in critical units (and at the present time) is denoted hereunder by $\Omega_{gw}(\nu) \equiv \Omega_{gw}(\nu, \tau_0)$ where ν is the comoving frequency. In the concordance paradigm $\Omega_{gw}(\nu)$ approximately scales as ν^{-2} between the aHz and 100 aHz [8, 9, 10] while it is flat (or slightly decreasing) for larger frequencies.

Two tacit assumptions are implicitly associated with r_T : the first one is that the early completion of the concordance paradigm is provided by the conventional inflationary scenario, the second is that the consistency relations are not violated⁴. Between these two assumptions (which are rarely stressed) the former seems stronger than the latter but they are instead equally essential if the only final objective is a stringent set of bounds on r_T from the temperature and polarization anisotropies of the microwave background. In practice the consistency relations stipulate that the tensor spectral index n_T and the slow-roll parameter ϵ are both determined by the value of r_T according to the following (approximate) chain of equalities $n_T \simeq -r_T/8 \simeq -2\epsilon$. The consistency relations are valid in the case of single-field inflationary scenarios (see e.g. [11]) but they can be otherwise broken. Since the vanilla Λ CDM only represents a useful compromise between the available data and the number of ascertainable parameters, the addition of a tensor component (only described by r_T) allows for a rather accurate set of limits implying, in a conservative perspective, that $r_T \leq 0.06$ [5, 6, 7]. If the consistency conditions are broken the accuracy on r_T becomes comparatively smaller and, for this reason, some time ago it has been suggested that the bounds on r_T must be viewed in a broader perspective where the analysis of the three standard cosmological data sets (i.e. cosmic microwave background anisotropies, large-scale structure and supernovae), is combined with the bounds of wide-band interferometers in the so-called audio band (i.e. between few Hz and few kHz) [12].

Since direct measurements are now available it seems appropriate to reconsider the high-frequency normalization of the cosmic backgrounds of relic gravitons as a possible alternative to the conventional approach based on the analysis of the aHz region. There are two complementary motivations corroborating this suggestion and they are associated with the recent claims of the pulsar timing arrays (PTA) in the nHz band and with the improved constraints provided by the wide-band interferometers in the audio band. Indeed, in the last thirty years the pulsars provided a series of relevant upper limits on the

² Λ stands for the dark-energy component while the CDM denotes the Cold Dark Matter contribution. The simplest scenario where the neutrinos are massless, the dark-energy does not fluctuate and the tensor modes are absent is customarily referred to as the vanilla Λ CDM model.

³The units $\hbar = c = 1$ will be consistently employed throughout. Furthermore in this investigation the scale factor is normalized as $a(\tau_0) = a_0 = 1$. Finally, the standard prefixes shall be consistently employed, e.g. $1 \text{ aHz} = 10^{-18} \text{ Hz}$, $1 \text{ mHz} = 10^{-3} \text{ Hz}$, $1 \text{ MHz} = 10^6 \text{ Hz}$ and so on and so forth.

⁴For the sake of conciseness the argument of $r_T(k)$ will be dropped when not strictly necessary and we shall therefore employ the following shorthand notation $r_T = r_T(k_p)$.

spectral energy density of the relic gravitons at intermediate frequencies [13, 14, 15, 16, 17]. Broadly speaking the previous results⁵ suggested $h_0^2 \Omega_{gw}(\nu, \tau_0) < 10^{-10}$ for $\nu = \nu_P = \mathcal{O}(\text{nHz})$. More recently the PTA reported a series of effects that could be attributed to the relic gravitons [18, 19, 20, 21]. Barring for the slight differences between results reported by the four collaborations, the current evidence might suggest that $h_0^2 \Omega_{gw}(\nu, \tau_0) = \mathcal{O}(10^{-9})$ for a narrow slice of frequencies approximately ranging between a fraction of the nHz and 30 nHz. The observations of Refs. [18, 19, 20, 21] are, at the moment, very preliminary and the key property of a PTA is that the signal from relic gravitons, unlike a potential noise, is correlated across the baselines. These correlations have not been observed but it is nonetheless interesting to consider more carefully the relic gravitons in the nHz domain; this is the perspective already conveyed some years ago [22, 23] before the evidences of the PTA. The potential signals in the nHz band must anyway be complemented by a series of more robust limits in the audio band coming from the direct measurements of wide-band detectors. Depending on the slope of the spectral energy density, the bounds from wide-band interferometers slowly improved through the years [24, 25, 26, 27, 28, 29, 30] and finally led to the joint analysis of the LIGO, Virgo and KAGRA collaborations [31] suggesting that we can even have $\Omega_{gw}(\nu, \tau_0) \leq \mathcal{O}(10^{-9})$ for typical frequencies between 20 Hz and 80 Hz. The current measurements in the nHz and in the audio band seem then to point towards a quasi-flat spectral energy density of the relic gravitons when the comoving frequency encompasses the nHz and the audio bands.

In this paper we argue that even in the context of conventional inflationary models, the spectral energy density of the relic gravitons can be quasi-flat at high-frequency with typical amplitudes much larger than the ones of the concordance scenario. The potential signal must then be compatible, in this context, with the PTA observations and consistent with the limits of wide-band interferometers in the audio band. Instead of worrying about r_T (as customarily done in the standard approach [5, 6, 7]) we can directly impose the high-frequency normalization⁶. To pursue this possibility we first propose a general four-dimensional action for the consistent analysis of the relic gravitons evolving in conformally flat background geometries and generalizing the Ford-Parker action of Ref. [3]. After introducing the different parametrizations of the action and its quantization, the conditions leading to a flat slope at high-frequency are analyzed by computing the spectral energy density within the Wentzel-Kramers-Brillouin (WKB). The strategy for the high-frequency normalization is then explained by considering the PTA evidences, the limits from the wide-band detectors and the other constraints customarily associated with the high-frequency gravitons. In short the layout of the paper is the following. In section 2 the basic action of the problem is analyzed in its different forms. As suggested by the current data, the normalization of the spectral energy density in the nHz and audio bands is discussed in section 3. Section 4 is focused on the conditions for a flat high-frequency spectrum with amplitudes potentially much larger than the signal of the vanilla Λ CDM scenario. In section 5 we present some phenomenological considerations that complement the results of section 4. Finally section 6 contains the concluding remarks.

⁵As usual h_0 is the Hubble rate expressed in units of 100 Hz km/Mpc and since $\Omega_{gw}(\nu)$ denotes the spectral energy density in critical units, h_0^2 appears in its denominator. For this reason it is common practice to phrase the discussions directly in terms of $h_0^2 \Omega_{gw}(\nu)$ that is independent of the specific value of h_0 .

⁶The approach discussed here does not exclude that r_T is drastically smaller than the current bounds stemming from the temperature and the polarization anisotropies of the microwave background.

2 General parametrization of the action

2.1 The general action and its parametrizations

In the single-field case the effective action of generic inflationary models involves all the terms that include four derivatives and are suppressed by the negative powers of a large mass scale [32]. In non-generic models of inflation the higher-order corrections may assume a specific form either because the inflaton has a particular symmetry or because the rate of inflaton roll remains constant (and possibly larger than 1). Examples along this direction are certain fast-roll scenarios [33, 34, 35] or the higher-order curvature corrections given in terms of the Gauss-Bonnet combination and weighted (in four space-time dimensions) by inflaton-dependent couplings [36, 37, 38]. Similar modifications of the evolution of the tensor modes occurs in the case of Einstein-aether models [39, 40, 41] or in the case of compact extra-dimensions [45, 46]. From the physical viewpoint a common aspect of different parametrizations is that the gravitational waves may acquire an effective index of refraction [22, 23], as suggested long ago [42, 43] without any reference to the inflationary dynamics (see also [44]). Even if the geometry undergoes a stage of conventional accelerated expansion the intermediate slope of the spectral energy density increases depending on the evolution of the refractive index [22, 23]. The different contributions to the evolution of the tensor modes of the geometry in the case of conformally flat background geometries are summarized as follows:

$$S_g = \frac{1}{8\ell_P^2} \int d^3x \int d\tau \left[A(\tau) \partial_\tau h_{ij} \partial_\tau h^{ij} - B(\tau) \partial_k h_{ij} \partial^k h^{ij} - B_c(\tau) \bar{\gamma}^{AB} \partial_A h_{ij} \partial_B h^{ij} \right]. \quad (2.1)$$

In Eq. (2.1) the terms that would break parity and that are associated with quadratic combinations involving either dual Riemann tensor or the dual Weyl tensor have been neglected; both terms would appear in the effective action [32] (see also [47]) and might in principle polarize the relic gravitons. Equation (2.1) contains three undetermined functions $A(\tau)$, $B(\tau)$ and $B_c(\tau)$. The coefficient $B(\tau)$ refers to the expanding dimensions while the presence of $B_c(\tau)$ is related to a possible mass term that arises from the internal (compact) dimensions⁷. In the case of a toroidal compactification (which is the one discussed here) $\bar{\gamma}_{AB} = \delta_{AB}$ [45, 46]. There are two equivalent ways in which Eq. (2.1) can be phrased in terms of an appropriate refractive index. The first possibility is to factor $A(\tau)$:

$$S_g = \frac{1}{8\ell_P^2} \int d^3x \int d\tau A(\tau) \left[\partial_\tau h_{ij} \partial_\tau h^{ij} - \frac{1}{n^2(\tau)} \partial_k h_{ij} \partial^k h^{ij} - \frac{1}{n_c^2(\tau)} \bar{\gamma}^{AB} \partial_A h_{ij} \partial_B h^{ij} \right], \quad (2.2)$$

where $n(\tau)$ and $n_c(\tau)$ denote the refractive indices associated, respectively, with the expanding and with the compact dimensions:

$$n(\tau) = \sqrt{A(\tau)/B(\tau)}, \quad n_c(\tau) = \sqrt{A(\tau)/B_c(\tau)}. \quad (2.3)$$

The explicit form of the action (2.3) simplifies by changing the time parametrization and by rescaling the background dependence:

$$S_g = \frac{1}{8\ell_P^2} \int d^3x \int d\eta c^2(\eta) \left[\partial_\eta h_{ij} \partial_\eta h^{ij} - \partial_k h_{ij} \partial^k h^{ij} - r_c^2(\eta) \bar{\gamma}^{AB} \partial_A h_{ij} \partial_B h^{ij} \right]. \quad (2.4)$$

⁷In this situation the reduced Planck length is a function of the volume of the internal dimensions. We will generally work with the case of a spatially flat internal and external manifold with topology $M_{3+1} \times T_d$ where $(3+1)$ is the conventional $(3+1)$ -dimensional flat Universe and T_d is the d -dimensional torus. In what follows the Latin (lowercase) indices refer to the 3 (external) dimensions while the Latin (uppercase) indices refer to the internal dimensions.

Equation (2.4) follows from Eq. (2.2) by changing the time parametrization and by redefining the background dependence according to:

$$n(\eta) d\eta = d\tau, \quad c(\eta) = \sqrt{A(\eta)/n(\eta)}, \quad r_c(\eta) = n(\eta)/n_c(\eta). \quad (2.5)$$

We could have made a different choice by factoring $B(\tau)$ instead of $A(\tau)$ in Eq. (2.1). This second choice is actually immaterial since the final result is exactly the same in the two cases. In fact if we first rescale $B(\tau)$ we simply get the analog of Eq. (2.2) which is:

$$S_g = \frac{1}{8\ell_P^2} \int d^3x \int d\tau B(\tau) \left[n^2(\tau) \partial_\tau h_{ij} \partial_\tau h^{ij} - \partial_k h_{ij} \partial^k h^{ij} - \frac{B_c(\tau)}{B(\tau)} \bar{\gamma}^{AB} \partial_A h_{ij} \partial_B h^{ij} \right]. \quad (2.6)$$

If we again introduce the η -time defined as $n(\eta) d\eta = d\tau$, Eq. (2.6) becomes

$$S_g = \frac{1}{8\ell_P^2} \int d^3x \int d\eta \bar{c}^2(\eta) \left[\partial_\eta h_{ij} \partial_\eta h^{ij} - \partial_k h_{ij} \partial^k h^{ij} - r_c^2(\eta) \bar{\gamma}^{AB} \partial_A h_{ij} \partial_B h^{ij} \right], \quad (2.7)$$

where $\bar{c}(\eta) = \sqrt{B(\eta)n(\eta)}$. By now comparing Eqs. (2.4) and (2.7) we see that $\bar{c}(\eta)$ and $c(\eta)$ coincide since, in both cases, $\bar{c}(\eta) = c(\eta) = [A(\eta)B(\eta)]^{1/4}$.

2.2 Quantization and spectra in the η -time parametrization

Since the two approaches mentioned above are equivalent we can introduce, as usual, the normal modes of the system $\mu_{ij}(\vec{x}, \eta) = c(\eta) h_{ij}(\vec{x}, \eta)$ so that the action takes the form:

$$\begin{aligned} S_g &= \frac{1}{8\ell_P^2} \int d^3x \int d\eta \left[\partial_\eta \mu_{ij} \partial_\eta \mu^{ij} + \mathcal{F}^2 \mu_{ij} \mu^{ij} - \mathcal{F} \left(\mu_{ij} \partial_\eta \mu^{ij} + \mu^{ij} \partial_\eta \mu_{ij} \right) \right. \\ &\quad \left. - \partial_k \mu_{ij} \partial^k \mu^{ij} - r^2(\eta) \bar{\gamma}^{AB} \partial_A \mu_{ij} \partial_B \mu^{ij} \right], \end{aligned} \quad (2.8)$$

where \mathcal{F} denotes the rate of variation of $c(\eta)$:

$$\mathcal{F} = \frac{\dot{c}}{c} = n \frac{c'}{c}, \quad \dot{} = \partial_\eta, \quad ' = \partial_\tau. \quad (2.9)$$

In Eq. (2.9) the overdot and the prime denote, respectively, a derivation with respect to η and with respect to τ . Three complementary time parametrizations are relevant for the present analysis and their features can be summarized, in short, as follows⁸. The η -time parametrization and the conformal time are related as $n(\eta) d\eta = d\tau$ (see also Eqs. (2.2)–(2.3)); the dictionary between the two is:

$$\mathcal{F} = \frac{\dot{c}}{c} = \frac{\partial \ln c}{\partial \eta} \equiv n a F, \quad F = \frac{\partial \ln c}{\partial t}. \quad (2.10)$$

The variation of the background geometry is typically expressed in terms of the cosmic time coordinate t that is related to τ as $a(\tau) d\tau = dt$ and, as usual, the connection between the rates of variation of the background is:

$$\mathcal{H} = \frac{a'}{a} = \frac{\partial \ln a}{\partial \tau} \equiv a H, \quad H = \frac{\partial \ln a}{\partial t}. \quad (2.11)$$

⁸Since the usual Hubble rate $H = \partial_t a/a$ is defined in the cosmic time parametrization we remind that the overdot often denotes the derivative with respect to the cosmic time coordinate t but, in the present context, the overdot will be reserved for the derivation with respect to η -time, as suggested in Eq. (2.9).

The rate of variation of the refractive index in units of the Hubble rate and the rate of variation of H itself are then defined as:

$$\alpha = \frac{\partial \ln n}{\partial \ln a} = \frac{1}{nH} \frac{\partial n}{\partial t}, \quad \epsilon = -\frac{\partial_t H}{H^2} \ll 1, \quad (2.12)$$

where ϵ is the usual slow-roll parameter. Since the phase velocity coincides with the group velocity, the refractive index must increase during inflation (i.e. $\alpha \geq 0$) to prevent a superluminal propagation of the signal; there are, in practice, two relevant physical situations depending on the value of α , i.e. $\alpha < 1$ and $\alpha = \mathcal{O}(1)$: in the first case α and ϵ are of the same order while in the second case $\alpha \gg \epsilon$. In what follows α is kept generic however, as we shall see, the tensor spectral index is determined by the competition of α and ϵ and the physical range corresponds to $\alpha < 1$. We finally remark, as already mentioned, that the conventional slow-roll dynamics does not necessarily imply the validity of the so-called consistency relations which are instead broken by the presence of the refractive index so that, the tensor spectral index and the tensor-to-scalar ratio are not solely determined by ϵ , as it happens when the consistency relations are enforced. After these necessary specifications we can define the canonical momenta from Eq. (2.8)

$$\pi_{ij} = \frac{1}{8\ell_P^2} \left[\dot{\mu}_{ij} - \mathcal{F} \mu_{ij} \right], \quad \pi^{ij} = \frac{1}{8\ell_P^2} \left[\dot{\mu}^{ij} - \mathcal{F} \mu^{ij} \right], \quad (2.13)$$

so that the canonical Hamiltonian becomes:

$$\begin{aligned} H_g(\eta) &= \int d^3x \left[8\ell_P^2 \pi_{ij} \pi^{ij} + \mathcal{F} \left(\mu_{ij} \pi^{ij} + \mu^{ij} \pi_{ij} \right) \right. \\ &\quad \left. + \frac{1}{8\ell_P^2} \partial_k \mu_{ij} \partial^k \mu^{ij} + \frac{r^2(\eta)}{8\ell_P^2} \bar{\gamma}^{AB} \partial_A \mu_{ij} \partial_B \mu^{ij} \right]. \end{aligned} \quad (2.14)$$

From Eq. (2.14) the Hamilton's equations are:

$$\dot{\mu}_{ij} = 8\ell_P^2 \pi_{ij} + \mathcal{F} \mu_{ij}, \quad \dot{\pi}_{ij} = -\mathcal{F} \pi_{ij} + \frac{\nabla^2 \mu_{ij}}{8\ell_P^2} + r^2 \frac{\bar{\nabla}^2 \mu_{ij}}{8\ell_P^2}, \quad (2.15)$$

where the Laplacian associated with the internal dimensions has been denoted by $\bar{\nabla}^2 = \bar{\gamma}^{AB} \partial_A \partial_B$. We can now quantize the system in the standard manner but, for the sake of accuracy, we repeat here the main steps. It is first useful to express the quantum field operators $\hat{\mu}_{ij}(\vec{x}, \eta)$ and $\hat{\pi}_{mn}(\vec{x}, \eta)$ directly in Fourier space:

$$\hat{\mu}_{ij}(\vec{q}, \eta) = \frac{1}{(2\pi)^{3/2}} \int d^3x e^{i\vec{q}\cdot\vec{x}} \hat{\mu}_{ij}(\vec{x}, \eta), \quad \hat{\pi}_{mn}(\vec{p}, \eta) = \frac{1}{(2\pi)^{3/2}} \int d^3x e^{i\vec{p}\cdot\vec{x}} \hat{\pi}_{mn}(\vec{x}, \eta). \quad (2.16)$$

The field operators in Fourier space can then be expanded in the basis of the two (linear) tensor polarizations⁹:

$$\hat{\mu}_{ij}(\vec{q}, \eta) = \sum_{\lambda=\oplus, \otimes} e_{ij}^{(\lambda)}(\hat{q}) \hat{\mu}_\lambda(q, \eta), \quad \hat{\pi}_{mn}(\vec{p}, \eta) = \sum_{\lambda=\oplus, \otimes} e_{mn}^{(\lambda)}(\hat{p}) \hat{\pi}_\lambda(p, \eta). \quad (2.17)$$

⁹The explicit form of the two linear polarizations is given by $e_{ij}^{(\oplus)}(\hat{k}) = (\hat{m}_i \hat{m}_j - \hat{n}_i \hat{n}_j)$ and by $e_{ij}^{(\otimes)}(\hat{k}) = (\hat{m}_i \hat{n}_j + \hat{n}_i \hat{m}_j)$ where $\hat{k}_i = k_i/|\vec{k}|$, \hat{m}_i and \hat{n}_i are three mutually orthogonal unit vectors obeying $\hat{m} \times \hat{n} = \hat{k}$.

The field operators of Eq. (2.17) can be directly written in terms of the creation and annihilation operators obeying $[\hat{a}_{\vec{q},\lambda}, \hat{a}_{\vec{p},\lambda}^\dagger] = \delta^{(3)}(\vec{q} - \vec{p})$ so that, ultimately, $\hat{\mu}_{ij}(\vec{q}, \eta)$ and $\hat{\pi}_{mn}(\vec{p}, \eta)$ are:

$$\hat{\mu}_{ij}(\vec{q}, \eta) = \sqrt{2}\ell_P \sum_{\lambda} \left[e_{ij}^{(\lambda)}(\hat{q}) f_{k,\lambda}(\eta) \hat{a}_{\vec{q}\lambda} + e_{ij}^{(\lambda)}(-\hat{q}) f_{k,\lambda}^*(\eta) \hat{a}_{-\vec{q}\lambda}^\dagger \right], \quad (2.18)$$

$$\hat{\pi}_{mn}(\vec{p}, \eta) = \frac{1}{4\sqrt{2}\ell_P} \sum_{\lambda} \left[e_{mn}^{(\lambda)}(\hat{p}) g_{k,\lambda}(\eta) \hat{a}_{\vec{p}\lambda} + e_{mn}^{(\lambda)}(-\hat{p}) g_{k,\lambda}^*(\eta) \hat{a}_{-\vec{p}\lambda}^\dagger \right]. \quad (2.19)$$

It can be directly checked that the commutation relations between $\hat{\mu}_{ij}(\vec{q}, \eta)$ and $\hat{\pi}_{mn}(\vec{p}, \eta)$ are given by:

$$[\hat{\mu}_{ij}(\vec{q}, \eta), \hat{\pi}_{mn}(\vec{p}, \eta)] = i \mathcal{S}_{ijmn}(\hat{q}) \delta^{(3)}(\vec{q} + \vec{p}), \quad (2.20)$$

where $\mathcal{S}_{ijmn}(\hat{q})$

$$\mathcal{S}_{ijmn}(\hat{q}) = \frac{1}{4} \left[p_{mi}(\hat{q}) p_{nj}(\hat{q}) + p_{mj}(\hat{q}) p_{ni}(\hat{q}) - p_{ij}(\hat{q}) p_{mn}(\hat{q}) \right], \quad (2.21)$$

and $p_{ij} = (\delta_{ij} - \hat{q}_i \hat{q}_j)$. Note that Eq. (2.20) holds provided the Wronskian normalization condition is verified:

$$f_{q,\lambda}(\eta) g_{q,\lambda}^*(\eta) - f_{q,\lambda}^*(\eta) g_{q,\lambda}(\eta) = i. \quad (2.22)$$

It is finally practical to deduce the two-point functions of $\hat{h}_{ij}(\vec{k}, \eta)$ and of $\partial_\eta \hat{h}_{ij}(\vec{k}, \eta)$ in Fourier space:

$$\langle \hat{h}_{ij}(\vec{k}, \eta) \hat{h}_{mn}(\vec{p}, \eta) \rangle = \frac{2\pi^2}{k^3} P_T(k, \eta) \mathcal{S}_{ijmn}(\hat{k}) \delta^{(3)}(\vec{k} + \vec{p}), \quad (2.23)$$

$$\langle \partial_\eta \hat{h}_{ij}(\vec{k}, \eta) \partial_\eta \hat{h}_{mn}(\vec{p}, \eta) \rangle = \frac{2\pi^2}{k^3} Q_T(k, \eta) \mathcal{S}_{ijmn}(\hat{k}) \delta^{(3)}(\vec{k} + \vec{p}), \quad (2.24)$$

where the power spectra $P_T(k, \tau)$ and $Q_T(k, \tau)$ are defined, respectively, by:

$$P_T(k, \eta) = \frac{4\ell_P^2 k^3}{\pi^2 c^2(\eta)} |f_k(\eta)|^2, \quad Q_T(k, \eta) = \frac{4\ell_P^2 k^3}{\pi^2 c^2(\eta)} |g_k(\eta)|^2. \quad (2.25)$$

All in all, putting everything together, we have that the field operators are expressed as:

$$\hat{\mu}_{ij}(\vec{x}, \eta) = \frac{\sqrt{2}\ell_P}{(2\pi)^{3/2}} \sum_{\lambda=\oplus, \otimes} \int d^3k e_{ij}^{(\lambda)}(\vec{k}) \left[f_{k,\lambda}(\eta) \hat{a}_{\vec{k}\lambda} e^{-i\vec{k}\cdot\vec{x}} + f_{k,\lambda}^*(\eta) \hat{a}_{\vec{k}\lambda}^\dagger e^{i\vec{k}\cdot\vec{x}} \right], \quad (2.26)$$

$$\hat{\pi}_{ij}(\vec{x}, \eta) = \frac{1}{4\sqrt{2}\ell_P (2\pi)^{3/2}} \sum_{\lambda=\oplus, \otimes} \int d^3k e_{ij}^{(\lambda)}(\vec{k}) \left[g_{k,\lambda}(\eta) \hat{a}_{\vec{k}\lambda} e^{-i\vec{k}\cdot\vec{x}} + g_{k,\lambda}^*(\eta) \hat{a}_{\vec{k}\lambda}^\dagger e^{i\vec{k}\cdot\vec{x}} \right], \quad (2.27)$$

where, according to Eq. (2.15), the evolution of the mode functions $f_{k,\lambda}$ and $g_{k,\lambda}$ obeys:

$$\dot{f}_{k,\lambda} = g_{k,\lambda} + \mathcal{F} f_{k,\lambda}, \quad (2.28)$$

$$\dot{g}_{k,\lambda} = -k^2 f_{k,\lambda} - \mathcal{F} f_{k,\lambda} - q^2 r^2 f_{k,\lambda}. \quad (2.29)$$

Thanks to the coupling among the scalar and the tensor modes the gravity wave evolution equation get what looks like a massive contribution [45, 46]. In terms of the eigenstates of the Laplace operators appearing in Eq. (2.15) we have that $\nabla^2 \mu_{ij} = -k^2 \mu_{ij}$ and $\bar{\nabla}^2 \mu_{ij} = -q^2 \mu_{ij}$. While k denotes the external momentum, q is the momentum associated with the extra-dimensions which can be viewed as a massive contribution as it can be appreciated by decoupling Eqs. (2.28)–(2.29):

$$\ddot{f}_k + \left[k^2 + q^2 r^2 - \frac{\ddot{c}}{c} \right] f_k = 0, \quad g_k = \dot{f}_k - \mathcal{F} f_k; \quad (2.30)$$

the polarization index has been omitted since the result of Eq. (2.33) holds both for \oplus and for \otimes .

2.3 Different physical limits

Depending on the values of $c(\eta)$, $n(\eta)$ and $r(\eta)$, the action of Eq. (2.8) describes a number of relevant situations that are however physically different. In the standard limit the refractive index is absent and the internal dimensions disappear:

$$n \rightarrow 1, \quad r \rightarrow 0, \quad \eta \rightarrow \tau, \quad c(\tau) = a(\tau), \quad (2.31)$$

In the limit (2.31) the rescaled normal mode becomes $\mu_{ij} = a(\tau)h_{ij}$ and $a(\tau)$ is the scale factor appearing in the four-dimensional line element

$$ds^2 = \bar{g}_{\mu\nu} dx^\mu dx^\nu, \quad \bar{g}_{\mu\nu} = a^2(\tau)\eta_{\mu\nu}, \quad (2.32)$$

where $\eta_{\mu\nu}$ is the Minkowski metric. According to Eq. (2.8) coincides with the original Ford-Parker action [3]; furthermore, as stressed in Eq. (2.31), the η -time and the conformal time coordinates coincide. In the case of Eq. (2.31) the only possibility of getting a flat spectrum at high-frequency is to modify the standard inflationary dynamics by considering, for instance, the possibility of bouncing backgrounds. In this case Eq. (2.30) becomes:

$$f_k'' + \left[k^2 - \frac{a''}{a} \right] f_k = 0, \quad g_k = f_k' - \mathcal{H} f_k. \quad (2.33)$$

Let us now suppose that $n \rightarrow 1$ in the presence of d internal dimensions characterized by the scale factor $b^2(\tau)$ so that the line element is given by:

$$ds^2 = a^2(\tau)[d\tau^2 - d\vec{x}^2] - b^2(\tau)\bar{\gamma}^{AB} dy_A dy_B, \quad (2.34)$$

where $A, B = 1, \dots, d$ runs over the d internal dimensions and the dimensionality of the space-time is $D = 4 + d$. As already suggested, we mainly consider the case $\bar{\gamma}_{AB} = \delta_{AB}$. In the case of Eq. (2.34) the internal volume is $b^{d/2}$ and we then have that the various parameters

$$n \rightarrow 1, \quad r \rightarrow \frac{a(\tau)}{b(\tau)}, \quad \eta \rightarrow \tau, \quad c(\tau) = a(\tau) b^{d/2}(\tau). \quad (2.35)$$

In the situation of Eq. (2.35) the conformal time coincides with the η -time but the presence of $b(\tau)$ accounts for the dynamics of the d -extra-dimensions. According to Eq. (2.35) the explicit form of Eq. (2.30) becomes

$$f_k'' + \left[k^2 + q^2 \frac{a^2}{b^2} - \frac{(a b^{d/2})''}{a b^{d/2}} \right] f_k = 0, \quad g_k = f_k' - \mathcal{F} f_k, \quad \mathcal{F} = \mathcal{H} + \frac{d}{2} \frac{b'}{b}. \quad (2.36)$$

A scenario of dimensional decoupling based on Eq. (2.36) has been discussed in Refs. [45, 46] and the considerations reported here can be easily extended to that situation. We finally consider the framework that is more realistic, at least for the present ends:

$$r \rightarrow 0, \quad n(\eta)d\eta = d\tau, \quad c(\eta) = \frac{a(\eta)}{\sqrt{n(\eta)}}. \quad (2.37)$$

In the limit (2.37) the evolution of the mode functions (see Eq. (2.30)) becomes:

$$\ddot{f}_k + \left[k^2 - \frac{\ddot{c}}{c} \right] f_k = 0, \quad g_k = \dot{f}_k - \mathcal{F} f_k. \quad (2.38)$$

In the present discussion we also assume that the refractive index is exactly 1 at the present time. It is useful to remark that the evolution of the refractive index is specified unambiguously by assigning $n(a)$. Even though the phase velocity of the relic gravitons is not required to be sub-luminal we consider here the situation where $n(a) \geq 1$. When $n(a)$ changes appreciably during inflation and it goes to 1 in the standard decelerated stage of expansion¹⁰:

$$n(a) = n_* \frac{(a/a_*)^\alpha e^{-\gamma(a/a_*)}}{(a/a_*)^\alpha + 1} + 1, \quad n_* = n_i (a_*/a_i)^\alpha = n_i e^{\alpha N_*}. \quad (2.39)$$

Equation (2.39) defines, in practice, three successive physical regimes. For $a \gg a_1$ the refractive index goes to 1 and the standard situation is recovered depending on the value of $\gamma \geq 1$ which controls the sharpness of the transition. When $a_* < a < a_1$ the refractive index is practically constant but still larger than 1, i.e. $n(a) \simeq n_* > 1$. Finally for $a < a_*$ we have the truly refractive stage where $n(a) \simeq n_* (a/a_*)^\alpha$.

2.4 Chirp amplitude, spectral amplitude and spectral energy density

When discussing the relic gravitons at the present time the observational collaborations typically assume that the space-time is flat and that the frequency of the gravitons is always larger than the rate of variation of the geometry which means, in terms of the previous notations, that $k\eta \gg 1$. When we are in flat space-time and under the conditions of Eq. (2.39) we have that the conformal, the cosmic and the η -time all coincide at the present epoch i.e.

$$\eta = \tau = t, \quad c_0 = a_0 = 1. \quad (2.40)$$

Furthermore, since the scale factor is normalized to 1, the comoving and the physical frequencies are (today) coincident. To introduce the spectral amplitude the simplest approach is to expand the tensor amplitude as

$$h_{ij}(\vec{x}, \eta) = \int_{-\infty}^{\infty} d\nu \int d\hat{k} e^{2i\pi\nu(\eta - \hat{k}\cdot\vec{x})} h_{ij}(\nu, \hat{k}), \quad h_{ij}^*(\nu, \hat{k}) = h_{ij}(-\nu, \hat{k}), \quad (2.41)$$

where $\nu = k/(2\pi)$ is the comoving frequency and $d\hat{k} = d\cos\vartheta d\varphi$. As before $h_{ij}(\nu, \hat{k})$ can be expanded in the basis of the linear polarisations \oplus and \otimes :

$$h_{ij}(\nu, \hat{k}) = \sum_{\lambda=\oplus, \otimes} e_{ij}^{(\lambda)}(\hat{k}) h_\lambda(\nu, \hat{k}). \quad (2.42)$$

The spectral amplitude $S_h(|\nu|)$ is defined as the expectation value of the tensor amplitudes expressed as a function of ν and \hat{k} :

$$\langle h_\lambda(\nu, \hat{k}) h_{\lambda'}(\nu', \hat{k}') \rangle = \mathcal{A}_c S_h(|\nu|) \delta(\nu + \nu') \delta^{(2)}(\hat{k} - \hat{k}') \delta_{\lambda\lambda'}; \quad (2.43)$$

where \mathcal{A}_c is an overall constant that parametrizes the different choices currently adopted by different authors¹¹. Consistently with the previous notations, the angular delta function appearing in Eq.

¹⁰In Eq. (2.39) a_i and a_1 mark, respectively, the beginning and the end of the inflationary epoch; a_* defines the boundary of the refractive stage and N_* is the corresponding number of e -folds.

¹¹In the definition of the spectral amplitude we introduced a modulus since we intend to express the various integrations for positive values of ν .

(2.43) is given by $\delta^{(2)}(\widehat{k} - \widehat{k}') = \delta(\varphi - \varphi') \delta(\cos \vartheta - \cos \vartheta')$. If we now compute the expectation value of two tensor amplitudes with different indices we obtain

$$\langle h_{ij}(\nu, \widehat{k}) h_{\ell m}(\nu', \widehat{k}') \rangle = 4 \mathcal{A}_c \mathcal{S}_{ij\ell m}(\widehat{k}) S_h(|\nu|) \delta^{(2)}(\widehat{k} - \widehat{k}') \delta(\nu + \nu'), \quad (2.44)$$

where $\mathcal{S}_{ij\ell m}(\widehat{k})$ has been already introduced in Eq. (2.21). The expectation value of the tensor amplitudes at equal time becomes:

$$\begin{aligned} \langle h_{ij}(\vec{x}, \eta) h^{ij}(\vec{y}, \eta) \rangle &= \int_{-\infty}^{+\infty} d\nu \int_{-\infty}^{+\infty} d\nu' \int d\widehat{k} \int d\widehat{k}' \\ &\times e^{2i\pi\nu(\tau - \widehat{k} \cdot \vec{x})} e^{2i\pi\nu'(\tau - \widehat{k}' \cdot \vec{y})} \langle h_{ij}(\nu, \widehat{k}) h^{ij}(\nu', \widehat{k}') \rangle. \end{aligned} \quad (2.45)$$

The expectation value appearing in Eq. (2.45) can be directly computed thanks to Eqs. (2.44). More specifically, since $\mathcal{S}_{ijij} = 1$ Eq. (2.45) becomes:

$$\langle h_{ij}(\vec{x}, \eta) h^{ij}(\vec{y}, \eta) \rangle = 32\pi \mathcal{A}_c \int_0^\infty d\nu S_h(|\nu|) j_0(2\pi\nu r). \quad (2.46)$$

From the direct comparison of Eq. (2.46) with the analog expression computed in terms of $P_T(\nu)$ it follows that the relations between the chirp amplitude, the spectral amplitude and the power spectrum is:

$$h_c^2(\nu) = 16\pi \mathcal{A}_c \nu S_h(|\nu|), \quad P_T(\nu) = 32\pi \mathcal{A}_c \nu S_h(|\nu|). \quad (2.47)$$

The specific values of \mathcal{A}_c can be used to rationalize the obtained expressions. The LIGO/Virgo collaboration is normally setting $\mathcal{A}_c = 1/(16\pi)$ so that Eq. (2.47) becomes

$$h_c^2(\nu) = \nu S_h(|\nu|), \quad P_T(\nu) = 2\nu S_h(|\nu|), \quad \langle h_{ij}(\vec{x}, \tau) h^{ij}(\vec{x}, \tau) \rangle = 2 \int_0^\infty d\nu S_h(|\nu|). \quad (2.48)$$

The PTA collaborations express their results in terms of the chirp amplitude $h_c^2(\nu)$. In this respect we just note that, up to a numerical factor, the square of the chirp amplitude coincides with the power spectrum so that its relation with the spectral energy density may be easily determined and it is:

$$P_T(\nu, \tau_0) = 2 h_c^2(\nu, \tau_0), \quad \Omega_{gw}(\nu, \tau_0) = \frac{2\pi^2}{3H_0^2} \nu^2 h_c^2(\nu, \tau_0). \quad (2.49)$$

3 Normalization in the audio band and in the nHz domain

3.1 Wide-band interferometers and the audio band

The observations of wide-band detectors led through the years to a number direct upper limits on the backgrounds of relic gravitons for a frequency interval ranging between few Hz and 10 kHz [24, 25, 26, 27, 28, 29, 30, 31]. The most relevant upper limits are summarized in Tab. 1 and they depend on the spectral slope of the signal. For the purposes of Tab. 1 the spectral energy density has been parametrized with a power-law slope of the type:

$$\Omega_{gw}(\nu) = \bar{\Omega}(\sigma) \left(\frac{\nu}{\nu_{ref}} \right)^\sigma, \quad \sigma \geq 0, \quad (3.1)$$

Table 1: List of the direct limits on the relic gravitons obtained by wide-band interferometers.

Year	frequency range [Hz]	Bound	Reference
2004	40 – 314	$\bar{\Omega}(0) < 23$	Ref. [24]
2005	69 – 156	$\bar{\Omega}(0) < 8.4 \times 10^{-4}$	Ref. [25]
2012	600 – 1000	$\bar{\Omega}(3) < 0.32$	Ref. [26]
2014	41.5 – 169.25	$\bar{\Omega}(0) < 5.6 \times 10^{-6}$	Ref. [27]
2014	600 – 1000	$\bar{\Omega}(3) < 0.14$	Ref. [27]
2014	170 – 600	$\bar{\Omega}(0) < 1.8 \times 10^{-4}$	Ref. [27]
2014	1000 – 1726	$\bar{\Omega}(3) < 1$	Ref. [27]
2015	460 – 1000	$\bar{\Omega}(3) < 7.7 \times 10^{-4}$	Ref. [28]
2017	20 – 86	$\bar{\Omega}(0) < 1.7 \times 10^{-7}$	Ref. [29]
2017	20 – 300	$\bar{\Omega}(3) < 1.7 \times 10^{-8}$	Ref. [29]
2019	20 – 81.9	$\bar{\Omega}(0) < 6 \times 10^{-8}$	Ref. [30]
2019	20 – 95.2	$\bar{\Omega}(2/3) < 4.8 \times 10^{-8}$	Ref. [30]
2019	20 – 301	$\bar{\Omega}(3) < 7.9 \times 10^{-9}$	Ref. [30]
2021	20 – 76.6	$\bar{\Omega}(0) < 5.8 \times 10^{-9}$	Ref. [31]
2021	20 – 90.6	$\bar{\Omega}(2/3) < 3.4 \times 10^{-9}$	Ref. [31]
2021	20 – 291.6	$\bar{\Omega}(3) < 3.9 \times 10^{-10}$	Ref. [31]

where ν_{ref} is a (conventional) frequency while $\bar{\Omega}(\sigma)$ is the constant amplitude that differs¹² depending on the slope σ . The results of Tab. 1 show that the constant amplitudes associated with the various σ are constrained at different levels. The scale-invariant limit represents the simplest signal grossly compatible with the concordance paradigm; conversely, if $\sigma = 3$ in Eq. (3.1), the factor $\Omega_{gw}(\nu)^2/\nu^6$ is practically constant and, in this case, the estimate of the integral appearing in the signal-to-noise ratio gets simpler (see e.g. [49, 50, 51, 52]). In Refs.[24, 25, 26, 27, 28, 29] the LIGO/Virgo collaboration presented the upper limits for $\Omega(0)$ and $\Omega(3)$; a third case has been subsequently analyzed and it corresponds to $\sigma = 2/3$ [30, 31]. In the case of an exactly scale-invariant spectrum the constraints obtained in Refs. [29, 30] imply that $\bar{\Omega}(0) < 6 \times 10^{-8}$. If this value is compared with the analog result obtained in Ref. [27], the upper limit is $\mathcal{O}(100)$ times more constraining for the same slope and for the same frequency band. For $\sigma = 2/3$ the constraints of Ref. [29] imply $\bar{\Omega}_{2/3} < 4.8 \times 10^{-8}$ with 95% confidence within the 20–95 Hz frequency band with $\nu_{ref} = 25$ Hz. The slope $\sigma = 2/3$ may actually parametrize a potentially interesting foreground for the relic gravitons¹³. The most constraining limit to date in the case $\sigma = 2/3$ has been obtained in Ref. [31] by the Kagra-Ligo-Virgo collaboration and it requires that $\bar{\Omega}(2/3) < 3.4 \times 10^{-9}$. The most constraining set of bounds appearing in Tab. 1

¹²For instance, $\bar{\Omega}(0)$ is the amplitude of the scale-invariant spectral energy density while $\bar{\Omega}(3)$ is the amplitude of a spectral energy density with cubic slope.

¹³Depending on the estimates, the rates of black hole mergers range from $\mathcal{O}(50)$ Gpc⁻³yr⁻¹ to $\mathcal{O}(300)$ Gpc⁻³yr⁻¹. If this is the case we can not only expect to have many more signals but also a stochastic foreground coming from unresolved sources of gravitational radiation.

corresponds to the one obtained by the LIGO, Virgo and KAGRA collaborations [31]. In the case of a flat spectral energy density the bound reads¹⁴:

$$\Omega_{gw}(\nu_L) < 5.8 \times 10^{-9}, \quad 20 \text{ Hz} < \nu_L < 76.6 \text{ Hz}, \quad (3.2)$$

where ν_L denotes the LIGO-Virgo-KAGRA frequency; we shall commonly refer to this limit as the LVK bound. Even if in Eq. (3.2) we just quoted the most constraining limit, the LIGO-Virgo-KAGRA collaboration actually reports a threefold bound for three different values of σ . When the value of σ increases the bound becomes more restrictive once the reference frequency is kept fixed. The three results are unified in the following interpolating formula

$$\log \bar{\Omega}(\sigma) < -8.236 - 0.335 \sigma - 0.018 \sigma^2. \quad (3.3)$$

that will be used to impose the LVK bound at high-frequency.

3.2 Pulsar timing arrays and the nHz band

Equations (3.2)–(3.3) are just the last result of the series of bounds given in Tab. 1 and it is not excluded they might be further improved in the near future. Already at the present stage, however, they are quite interesting if they are combined with the current evidences provided by the Pulsar Timing Arrays (PTA). In Tab. 2 we illustrate the main findings of the four different PTA collabora-

Table 2: List of current measurements from the various Pulsar Timing Arrays. The typical reference frequency is taken to be $\nu_{ref} = 31.68 \text{ nHz}$.

Experiment	q	β	$h_0^2 \Omega_{gw}(\nu_{ref}, \tau_0)$	Reference
Nanograv	1.92	$-2/3$	2.31×10^{-9}	Ref. [18]
PPTA	2.2	$-2/3$	3.04×10^{-9}	Ref. [19]
EPTA	2.95	$-2/3$	5.47×10^{-9}	Ref. [20]
EPTA	5.13	-0.33	1.65×10^{-8}	Ref. [20]
IPTA	2.8	$-2/3$	4.93×10^{-9}	Ref. [21]
IPTA	3.8	-0.5	9.08×10^{-9}	Ref. [21]

tions [18, 19, 20, 21]. Before going through the details we can already see that the determinations of the spectral energy density seem to be, naively, at the same level of the LVK bound but in a different frequency domain. The two results of Ref. [20] differ because of the different values of β and the same comment also holds in the case of Ref. [21]. The various PTA collaborations [18, 19, 20, 21] express the chirp amplitude at a pivot frequency $\nu_{ref} = 31.68 \text{ nHz}$ corresponding to yr^{-1} :

$$h_c(\nu) = Q \left(\frac{\nu}{\nu_{ref}} \right)^\beta, \quad \nu_{ref} = \frac{1}{\text{yr}} = 31.68 \text{ nHz}. \quad (3.4)$$

¹⁴In what follows, for the sake of conciseness, when the time dependence is suppressed it is understood that the corresponding quantity is evaluated at the present time. So, for instance, $\Omega_{gw}(\nu) = \Omega_{gw}(\nu, \tau_0)$, $h_c(\nu, \tau_0) = h_c(\nu)$ and so on and so forth.

The pivotal model analyzed so far assumes $\beta = -2/3$ and this is the case preferentially reported in Tab. 2. The EPTA [20] and IPTA [21] collaborations also consider a more general class of scenarios where Q and β vary simultaneously. For instance the EPTA finds that the most favoured model to be the common uncorrelated red noise described by $Q = 5.13_{-2.73}^{+4.20} \times 10^{-15}$ with $\bar{\gamma} = 3.78_{-0.59}^{+0.69}$ where we recall that, within the present notations, $\beta = (3 - \bar{\gamma})/2$. If the spectral index is instead fixed as $\bar{\gamma} = 13/3$ (i.e. $\beta = -2/3$) Ref. [20] suggests $Q = 2.95_{-0.72}^{+0.89} \times 10^{-15}$. We note that $\bar{\gamma}$ will not be employed hereunder and it is only mentioned for the sake of accuracy since some of the PTA collaborations introduce this notation which is a bit contrived from the viewpoint of the present discussion.

For the different estimates of Refs. [18, 19, 20, 21] the value of Q is always $\mathcal{O}(10^{-15})$ it is therefore useful to express $Q = q_0 \times 10^{-15}$. Using this notation and Eq. (3.4) the spectral energy density in the nHz band can be finally expressed as¹⁵:

$$h_0^2 \Omega_{gw}(\nu) = 6.290 \times 10^{-10} q_0^2 \left(\frac{\nu}{\nu_{ref}} \right)^{2+2\beta}. \quad (3.5)$$

The potential signal of the PTA recently reported evidence of a potential signal in the nHz band. Using the spectral energy density in critical units as a pivotal variable the features of this purported signal would imply, in the present notations, that:

$$10^{-9.88} < \frac{h_0^2 \Omega_{gw}(\nu_P)}{q_0^2} < 10^{-8.86}, \quad 3 \text{ nHz} < \nu_P < 100 \text{ nHz}. \quad (3.6)$$

3.3 Audio band and nHz band: which is the most restrictive?

To avoid potential confusions it is relevant to compare the limits in the audio band and in the nHz band to understand which are the most restrictive. Before discussing this comparison it is equally important to stress that the two classes of measurements are qualitatively different: while the limits from the audio band are specific to the case of relic gravitons [30, 31], the property of a PTA is that the signal from relic gravitons should be correlated across the baselines while that from the other noise will not. Since these correlations have not been observed so far, the interpretation suggested in by the PTA is still preliminary and the measurements of Refs. [18, 19, 20, 21] might not have anything to do with relic gravitons: the correlation signature of an isotropic gravitational wave background follows the so-called Hellings and Downs curve which depends on the angle between a pair of Earth-pulsars baselines. As already mentioned this correlation has not been observed yet by admission of the various experimental collaborations [18, 19, 20, 21]. If we assume that the PTA are indeed related with relic gravitons the constraint of Eqs. (3.2)–(3.3) is anyway more restrictive than the results of Eq. (3.6). Specialising, for simplicity, to the case of scale-invariant flat spectrum we have that from Eq. (3.2):

$$h_0^2 \Omega_{gw}(\nu_L) < 10^{-8.61} \left(\frac{h_0}{0.65} \right)^2, \quad (3.7)$$

where the limit has been referred to a fiducial value of h_0 that follows from the CMB data [5, 6, 7]. By comparing Eqs. (3.6) and (3.7) it seems that the former is superficially more constraining than the latter: by choosing $q_0 = 1$ we would have that $h_0^2 \Omega_{gw}(\nu) < 10^{-8.86}$. However q_0 is not 1; on the

¹⁵For instance the PPTA collaboration [19] suggests $q_0 = 2.2$; the IPTA estimates $q_0 = 2.8$ [21] while the EPTA [20] gives $q_0 = 2.95$. The results of PPTA, IPTA and EPTA seem, at the moment, to be broadly compatible with the NANOgrav 12.5 yrs data [18] implying $q_0 = 1.92$.

contrary if we take the average of the four measurements presented so far (see Tab. 2 in the case $\beta = -2/3$) we obtain an averaged value given by $\bar{q}_0 = 2.467$ which implies

$$10^{-9.09} \left(\frac{\bar{q}_0}{2.467} \right)^2 \leq h_0^2 \Omega_{gw}(\nu) \leq 10^{-8.07} \left(\frac{\bar{q}_0}{2.467} \right)^2. \quad (3.8)$$

Note that Eq. (3.7) is always *more* constraining than Eq. (3.8) even if we choose the smallest value of q_0 which is the one associated with the NANOgrav estimate [18]: if $q_0 = 1.92$ we get from Eq. (3.8) that $h_0^2 \Omega_{gw}(\nu) \leq 10^{-8.29}$ which is always larger than the value of Eq. (3.7). So far we simply considered the absolute values of the bounds but the frequency dependence of the theoretical spectra also matters: since $h_0^2 \Omega_{gw}(\nu, \tau_0)$ generally increases with ν , the limits of Eqs. (3.2) and (3.7) are comparatively even more constraining than the ones of Eqs. (3.6) and (3.8) for the simple reason that $\nu_L = \mathcal{O}(60)$ Hz while $\nu_P = \mathcal{O}(30)$ nHz. At high frequencies the limits of the audio band compete with the ones of nucleosynthesis (see the discussion hereunder). However if $h_0^2 \Omega_{gw}(\nu, \tau_0)$ is nearly scale-invariant the most constraining bounds remain the ones associated with Eqs. (3.2)–(3.3) and (3.7).

3.4 Big-bang nucleosynthesis limits

While the PTA measurements constrain the spectral energy density at intermediate frequencies, the bounds coming from big-bang nucleosynthesis [55, 56, 57] imply a constraint on the integral $h_0^2 \Omega_{gw}(\nu, \tau_0)$:

$$h_0^2 \int_{\nu_{bbn}}^{\nu_{max}} \Omega_{gw}(\nu, \tau_0) d \ln \nu = 5.61 \times 10^{-6} \Delta N_\nu \left(\frac{h_0^2 \Omega_{\gamma 0}}{2.47 \times 10^{-5}} \right), \quad (3.9)$$

where $\Omega_{\gamma 0}$ is the (present) critical fraction of CMB photons. The limit of Eq. (3.9) sets an indirect constraint on the extra-relativistic species possibly present at the time of nucleosynthesis. Since Eq. (3.9) is relevant in the context of neutrino physics, the limit is often expressed for practical reasons in terms of ΔN_ν representing the contribution of supplementary neutrino species. The actual bounds on ΔN_ν range from $\Delta N_\nu \leq 0.2$ to $\Delta N_\nu \leq 1$; the integrated spectral density in Eq. (3.9) is thus between 10^{-6} and 10^{-5} . It is relevant to point out, as we shall see, that the upper limit of integration (labeled by ν_{max}) depends on the specific post-inflationary evolutions¹⁶. Conversely, the lower limit of integration in Eq. (3.9) is given by the frequency corresponding to the Hubble rate at the nucleosynthesis epoch:

$$\nu_{bbn} = 2.252 \times 10^{-11} \left(\frac{N_{eff}}{10.75} \right)^{1/4} \left(\frac{T_{bbn}}{\text{MeV}} \right) \left(\frac{h_0^2 \Omega_{R0}}{4.15 \times 10^{-5}} \right)^{1/4} \text{ Hz} \simeq 0.01 \text{ nHz}, \quad (3.10)$$

where N_{eff} denotes the effective number of relativistic degrees of freedom entering the total energy density of the plasma and T_{bbn} is the temperature of big-bang nucleosynthesis. We finally remark that the bound of Eq. (3.9) could be relaxed if the nucleosynthesis takes place in the presence of matter-antimatter domains [56]. This possibility will not be specifically considered hereunder and we shall instead enforce the bound of Eqs. (3.9)–(3.10) in its conservative version. As we shall see when the quasi-flat spectrum is normalized in the audio band the limit (3.9) is always satisfied.

¹⁶In the forthcoming discussion an important element is the determination of ν_{max} that depends on the duration of the post-inflationary evolution and on the corresponding expansion rates. For $\nu > \nu_{max}$ the spectra of relic gravitons are exponentially suppressed since these wavelengths never cross the Hubble radius and are not amplified.

4 Conditions for flat spectra at high-frequency

In the conventional situation the spectral energy density for typical frequencies larger than the nHz is always smaller than 10^{-15} . If all the sources of late-time suppression are taken into account we approximately have $h_0^2 \Omega_{gw}(\nu) = \mathcal{O}(10^{-16.5})$. This conclusion can be however evaded in, at least, two complementary situations that are simultaneously illustrated in Fig. 1 where the common logarithm of $|\mathcal{F} = \dot{b}/b|$ is reported. The blobs appearing in the cartoon represent the transition regimes between

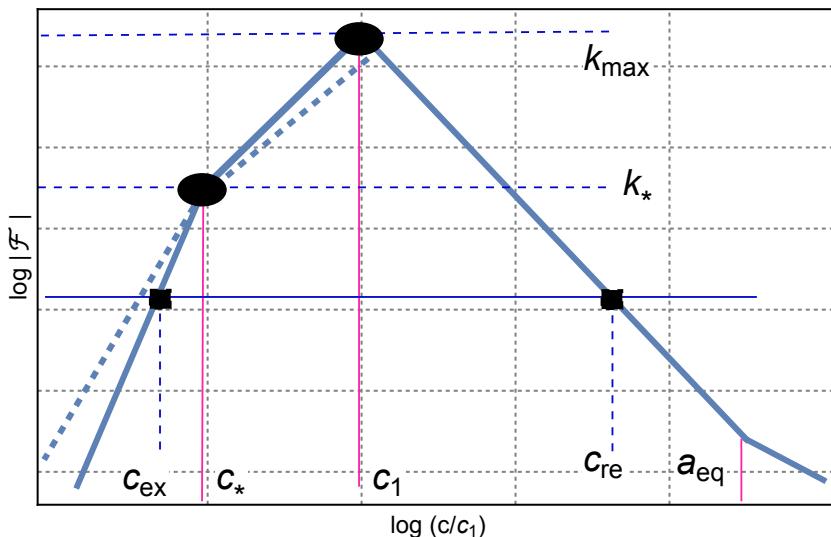


Figure 1: We schematically illustrate the evolution of \mathcal{F} when the conventional inflationary phase is preceded by a further evolutionary stage.

the different stages and they are immaterial in the approach based on WKB approximation that is adopted in the present section. Figure 1 illustrates two of the three limits discussed in Eqs. (2.31)–(2.35) and (2.37). In the case $n \rightarrow 1$ the η -time coincides with the conformal time coordinate and $\mathcal{F} = \mathcal{H} = aH$. Furthermore for $a > a_*$ the refractive index is not dynamical, and, in this limit, $c = a$. The most conservative case is the one associated with Eq. (2.37) where the refractive index evolves and we shall consider, in particular, the situation where $n(a)$ increases and then gets back to 1 for $c > c_*$ (see Eq. (2.39) and discussion therein).

For $k < k_*$ the amplitude and the slope of $\Omega_{gw}(k, \tau)$ depend on the profile of \mathcal{F} for $c < c_*$; this means that for $k_{eq} < k < k_*$, $\Omega_{gw}(k, \tau)$ increases provided the rate of variation of n is sufficiently large in Hubble units. In the language of Eq. (2.12) this implies $\alpha > 0$ even if, as we shall see, α cannot exceed 1 if the results of the wide band detectors are used to set the high-frequency normalization of the spectral energy density. According to Fig. 1 the spectral range $k_* < k < k_{max}$ is determined by the evolution of \mathcal{F} for $c_* < c < c_1$ where $\mathcal{F} \propto a^{-1}$. This scaling actually corresponds to the conventional situation since, in this interval, $\mathcal{F} \propto \mathcal{H} \simeq aH$ so that the Hubble rate is roughly constant. In the minimal situation where the refractive index flattens out for $c > c_*$ the spectral energy density is quasi-flat (or slightly decreasing) simply because, in this range, we get back to the conventional case where $\Omega_{gw}(k, \tau)$ is determined by the wavelengths crossing the Hubble radius during the inflationary stage and reentering when the background is dominated by radiation. Indeed for $c > c_1$ the evolution is completely standard and $\mathcal{F} = \mathcal{H} \propto a^{-1}$. Finally for $c > a_{eq}$ we have that $\mathcal{F} = \mathcal{H} \propto a^{-1/2}$. In

Fig. 1 we did not include the stage dominated by the dark energy simply because its contribution to the spectral energy density is immaterial for the considerations of this section. A more detailed account can be however found in section 5 where the late-time suppression of the spectral energy density will be more specifically investigated. For the normalization in the high-frequency regime it is useful to have a fairly general expression of the spectral energy density that can be deduced rather simply within the WKB approximation; a key role is played, in this context, by the structure of the turning points η_{ex} and η_{re} . As illustrated in Fig. 1, a generic wavenumber $k < k_{max}$ crosses $|\mathcal{F}(\eta)|$ twice in c_{ex} and c_{re} and these two values correspond to the moments where a given wavelength exists and reenters the effective Hubble radius $|\mathcal{F}(\eta)|^{-1}$. From a technical viewpoint η_{ex} and η_{re} are defined as the turning point at which the solution to Eq. (2.38) changes its analytic form. In particular the exit corresponds to:

$$k^2 = \left| \frac{\ddot{c}_{ex}}{c_{ex}} \right|, \quad \ddot{c}_{ex} \neq 0 \quad \Rightarrow \quad k = \sqrt{\left| \frac{\ddot{c}_{ex}}{c_{ex}} \right|}. \quad (4.1)$$

Equation (4.1) actually defines a regular turning point and it tells that, at η_{ex} , $k\eta_{ex} \simeq 1$. It can happen, however, that the turning point is singular and this happens, in particular, when $\ddot{c} \rightarrow 0$ in the vicinity of the turning point. In the problem at hand we have that $\ddot{c}_{ex} \neq 0$ however, if the reentry takes place during a radiation-dominated stage of expansion, we typically have $\ddot{c}_{re} \rightarrow 0$ since, in a radiation stage, $\eta = \tau$ and $a'' = 0$. In this case, as we shall see in a moment, we must recall that the condition $k\eta_{re} \simeq 1$ is not verified and it must be replaced by $k\eta_{re} \ll 1$. In what follows we shall first discuss the expression of the spectral energy density for the different ranges of wavelengths and then analyze the way the high-frequency normalization must be implemented.

4.1 Wavelengths larger than the effective horizon

To deduce the general evolution of the mode function for large wavelengths it is practical to transform the relevant differential equations in a set of integral equations. The evolution of the mode function of Eq. (2.38) is equivalent to¹⁷ an integral equation whose initial conditions are assigned at the reference time η_{ex} :

$$f_k(\eta) = \frac{c(\eta)}{c_{ex}} \left\{ f_k(\eta_{ex}) + g_k(\eta_{ex}) \int_{\eta_{ex}}^{\eta} \frac{c_{ex}^2}{c^2(\eta_1)} d\eta_1 - k^2 c_{ex} \int_{\eta_{ex}}^{\eta} \frac{d\eta_1}{c^2(\eta_1)} \int_{\eta_{ex}}^{\eta_1} c(\eta_2) f_k(\eta_2) d\eta_2 \right\}, \quad (4.2)$$

where, by definition, $c_{ex} = c(\eta_{ex})$. As argued in Eq. (4.1) the first turning point is always regular so that $k\eta_{ex} \simeq 1$. Neglecting then the terms $\mathcal{O}(k^2\eta^2)$ the lowest order solution of Eq. (4.2) is:

$$f_k(\eta) = \frac{c(\eta)}{c_{ex}} \left\{ f_k(\eta_{ex}) + g_k(\eta_{ex}) \int_{\eta_{ex}}^{\eta} \frac{c_{ex}^2}{c^2(\eta_1)} d\eta_1 \right\} + \mathcal{O}(k^2\eta^2). \quad (4.3)$$

Equation (4.3) determine the approximate form of the power spectrum for wavelengths larger than the Hubble radius. Since the second term appearing inside the squared bracket at the right hand side of Eq. (4.3) is subleading for typical wavelengths larger than the effective horizon, the explicit expression of the tensor power spectrum follows from Eq. (2.25) by recalling that, for $\eta < -\eta_*$,

$$c(\eta) = c_* (-\eta/\eta_*)^{-\zeta}, \quad \zeta = (2 - \alpha)/2(1 + \alpha - \epsilon), \quad c_* = a_*/\sqrt{n_*}. \quad (4.4)$$

¹⁷The same conclusion also holds in the case of Eq. (2.33) that is valid in the limit (2.31). The conditions (2.37) and (2.38) are actually more general than (2.31).

The expression of $c(\eta)$ follows, in its turn, from the definition of the η -time and from Eq. (2.39) evaluated in a conventional inflationary background with slow-roll rate given by ϵ . In the limit $|k\eta| \ll 1$ the tensor power spectrum is in fact constant and it is approximately given by:

$$P_T(k, \eta) = \frac{2\ell_P^2}{\pi^2 c_*^2 \eta_*^2} |A(\alpha, \epsilon)|^2 (-k\eta_*)^{n_T(\alpha, \epsilon)}, \quad k < k_*, \quad (4.5)$$

where $A(\alpha, \epsilon)$ and $n_T(\alpha, \epsilon)$ are defined, respectively, by:

$$n_T = \frac{3\alpha - 2\epsilon}{1 - \epsilon + \alpha}, \quad |A(\nu)| = \frac{\Gamma(\nu)}{\sqrt{\pi}} 2^{\nu-1/2}, \quad \nu = \frac{3 - \epsilon}{2(1 + \alpha - \epsilon)}. \quad (4.6)$$

Within the approximation scheme leading to Eq. (4.3) we have that in Eq. (4.5) $|A| = \sqrt{2k} |f_k(\eta_{ex})| = 1$. In a more general perspective the amplitude $|A|$ appearing in Eq. (4.5) parametrizes, up to an irrelevant phase, the mismatch between the exact and the approximate solutions at η_{ex} : for $k^2 \ll |\ddot{c}/c|$ the correctly normalized solutions of Eq. (2.33) are $f_k(\eta) = e^{\pm ik\eta}/\sqrt{2k}$. However as soon as η_{ex} is approached the amplitude gets slightly modified and the exact solution of Eq. (2.33) is given in terms of Hankel functions [53, 54]. The power spectrum of Eq. (4.5) can be further simplified by observing that:

$$\frac{1}{\eta_*^2} = \frac{n_*^2}{\tau_*^2} \left| 1 - \frac{\alpha}{1 - \epsilon} \right|^2 \quad \Rightarrow \quad \frac{1}{\eta_*^2} = a_*^2 n_*^2 H_*^2 \left| 1 - \frac{\alpha}{1 - \epsilon} \right|^2. \quad (4.7)$$

If we now use Eqs. (4.6)–(4.7) into Eqs. (4.5) we obtain the following form of the power spectrum for $k < a_* H_*$

$$P_T(k, \eta_*) = \left(\frac{H_*}{M_P} \right)^2 \frac{2^{6-n_T}}{\pi^2} \Gamma^2 \left(\frac{3-n_T}{2} \right) n_*^{3-n_T} \left| 1 + \frac{\alpha}{1 - \epsilon} \right|^{2-n_T} \left(\frac{k}{a_* H_*} \right)^{n_T}. \quad (4.8)$$

For the modes $k > a_* H_*$ the spectrum (4.8) is modified since now the evolution of the mode functions is given by:

$$f_k'' + \left[\omega^2 - \frac{a''}{a} \right] f_k = 0, \quad \omega^2 = k^2/n_*^2. \quad (4.9)$$

Recalling that $a''/a = a^2 H^2 (2 - \epsilon)$ and that $aH = -1/[(1 - \epsilon)\tau]$ Eq. (4.9) becomes

$$f_k'' + \left[\omega^2 - \frac{3 - \epsilon}{2(1 - \epsilon)^2} \right] f_k = 0, \quad (4.10)$$

If the refractive phase terminates before the end of inflation the power spectrum inherits a further branch for $a_* H_* < k \leq a_1 H_1$:

$$P_T(k, \tau_1) = \left(\frac{H_1}{M_P} \right)^2 n_*^{3-m_T} \frac{2^{6-m_T}}{\pi^2} \Gamma^2 \left(\frac{3-m_T}{2} \right) \left(\frac{k}{a_1 H_1} \right)^{m_T}, \quad m_T = -2\epsilon/(1 - \epsilon). \quad (4.11)$$

4.2 Wavelengths shorter than the effective horizon

All the cosmic gravitons measured at the present time are inside the Hubble radius and provided the reentry occurs when $\ddot{c}_{re} \neq 0$ we have that, approximately, $k\eta_{re} = \mathcal{O}(1)$. Conversely if $\ddot{b}_{re} \rightarrow 0$ in the vicinity of the turning point, then $k\eta_{re} \ll 1$. For $\eta \geq \eta_{re}$ the solution of Eq. (2.33) is

$$f_k(\eta) = \mathcal{C}_+(k, \eta_{ex}, \eta_{re}) \bar{f}_{re}(\eta) + \mathcal{C}_-(k, \eta_{ex}, \eta_{re}) \bar{f}_{re}^*(\eta), \quad (4.12)$$

where $\bar{f}_{re}(\eta)$ are the mode functions inside the effective horizon (i.e. $e^{-ik\eta}/\sqrt{2k}$ in the crudest approximation). The coefficients $\mathcal{C}_{\pm}(k, \eta_{ex}, \eta_{re})$ are

$$\begin{aligned}\mathcal{C}_{\pm}(k, \eta_{ex}, \eta_{re}) &= \frac{e^{-ik(\eta_{ex} \mp \eta_{re})}}{2ik} \left[\pm \frac{c_{ex}}{c_{re}} (\mathcal{F}_{ex} + ik) \mp \frac{c_{re}}{c_{ex}} (\mathcal{F}_{re} \mp ik) \right. \\ &\quad \left. \pm c_{re} c_{ex} (\mathcal{F}_{ex} + ik) (\mathcal{F}_{re} \mp ik) \mathcal{J}(\eta_{ex}, \eta_{re}) \right], \\ \mathcal{J}(\eta_{ex}, \eta_{re}) &= \int_{\eta_{ex}}^{\eta_{re}} \frac{d\eta}{c^2(\eta)}.\end{aligned}\tag{4.13}$$

If the reentry takes place, as we are considering here, when the refractive index is not dynamical, Eq. (4.13) can be simplified even further since $b(\eta) \rightarrow a(\tau)$ and $\mathcal{F} \rightarrow \mathcal{H}$:

$$\begin{aligned}\mathcal{C}_{\pm}(k, \eta_{ex}, \tau_{re}) &= \frac{e^{-ik(\eta_{ex} \mp \tau_{re})}}{2ik} \left[\pm \frac{c_{ex}}{a_{re}} (\mathcal{F}_{ex} + ik) \mp \frac{a_{re}}{c_{ex}} (\mathcal{H}_{re} \mp ik) \right. \\ &\quad \left. \pm a_{re} c_{ex} (\mathcal{F}_{ex} + ik) (\mathcal{H}_{re} \mp ik) \mathcal{J}(\eta_{ex}, \eta_{re}) \right],\end{aligned}\tag{4.14}$$

$$\mathcal{J}(\eta_{ex}, \tau_{re}) = \int_{\eta_{ex}}^{-\tau_1} \frac{d\eta}{c^2(\eta)} + \int_{-\tau_1}^{\tau_{re}} \frac{d\eta}{a^2(\tau)},\tag{4.15}$$

where $-\tau_1$ marks, as before, the end of the inflationary stage. Because $c(\eta)$ always increases, in Eqs. (4.14)–(4.15) the terms proportional to $|c_{ex}/c_{re}|$ can be neglected in comparison with $|b_{re}/b_{ex}|$. Since $\mathcal{C}_{\pm}(k)$ are both complex but subjected to the condition $|\mathcal{C}_+(k, \eta_{ex}, \eta_{re})|^2 - |\mathcal{C}_-(k, \eta_{ex}, \eta_{re})|^2 = 1$ it is sufficient to estimate the approximate form of $|\mathcal{C}_-(k, \eta_{ex}, \eta_{re})|^2$:

$$|\mathcal{C}_-(k, \eta_{ex}, \eta_{re})|^2 \simeq \frac{1}{4} \left(\frac{c_{re}}{c_{ex}} \right)^2 \left(1 + \frac{\mathcal{F}_{re}^2}{k^2} \right) \left[1 - 2\mathcal{F}_{ex} c_{ex}^2 \mathcal{J}(\eta_{ex}, \eta_{re}) + c_{ex}^4 (\mathcal{F}_{ex}^2 + k^2) \mathcal{J}^2(\eta_{ex}, \eta_{re}) \right].\tag{4.16}$$

Equation (4.16) allows for a swift determination of the power spectrum and of the spectral energy distribution in the limit $k\tau \gg 1$, i.e. when the relevant wavelengths are all inside the Hubble radius:

$$P_T(k, \tau) = \frac{4k^2}{\pi^2 \bar{M}_P^2 a^2} |\mathcal{C}_-(k, \eta_{ex}, \eta_{re})|^2 \left[1 + \mathcal{O}\left(\frac{1}{k^2 \tau^2}\right) \right],\tag{4.17}$$

$$\Omega_{gw}(k, \tau) = \frac{k^4}{3H^2 \bar{M}_P^2 \pi^2 a^4} |\mathcal{C}_-(k, \eta_{ex}, \eta_{re})|^2 \left[1 + \mathcal{O}\left(\frac{1}{k^2 \tau^2}\right) \right],\tag{4.18}$$

From the ratio between Eqs. (4.17)–(4.18) the standard relation between the power spectrum and the spectral energy density is recovered

$$\Omega_{gw}(k, \tau) = \frac{k^2}{12a^2 H^2} P_T(k, \tau) \left[1 + \mathcal{O}\left(\frac{1}{k^2 \tau^2}\right) \right],\tag{4.19}$$

and it is generally valid when the relevant wavelengths are shorter than the Hubble radius at a given epoch. Inside the Hubble radius we can evaluate indifferently either the power spectrum or the spectral energy distribution. It is finally useful to estimate more explicitly k_* and k_{max} . Since $k_* = 1/\eta_*$ we also have that

$$k_* = \left| 1 + \frac{\alpha}{1 - \epsilon} \right| e^{\alpha N_*} e^{-\Delta N} k_{max}, \quad \Delta N = N_t - N_*.\tag{4.20}$$

As usual in Eq. (4.20) $N_* = \ln(a_*/a_i)$ denotes the number of e -folds during the refractive stage $N_t = \ln(a_1/a_i)$ is the total number of e -folds. Recalling that $\nu_{max} = k_{max}/(2\pi)$ we then have, in explicit terms:

$$\nu_{max} = 269.33 \left(\frac{\epsilon}{0.003} \right)^{1/4} \left(\frac{\mathcal{A}_{\mathcal{R}}}{2.41 \times 10^{-9}} \right)^{1/4} \left(\frac{h_0^2 \Omega_{R0}}{4.15 \times 10^{-5}} \right)^{1/4} \text{ MHz}, \quad (4.21)$$

where $\mathcal{A}_{\mathcal{R}}$ is the amplitude of the scalar power spectrum at the pivot scale $k_p = 0.002 \text{ Mpc}^{-1}$ and Ω_{R0} is the total fraction of relativistic species at the present time in the concordance paradigm. Thanks to Eq. (4.20) we also have, by definition, that

$$\nu_* = \left(1 + \frac{\alpha}{1 - \epsilon} \right) e^{\alpha N_*} e^{-\Delta N} \nu_{max}. \quad (4.22)$$

We note that in Eq. (4.21) we introduced the slow-roll parameter ϵ and not r_T since we did not assume the consistency relations so that r_T might be smaller (or even much smaller) than 0.06.

4.3 Flat spectra at high frequencies

The spectral energy density for typical wavenumbers $a_* H_* < k < a_1 H_1$ is quasi-flat and to show this point in general terms it is useful to go back to Eqs. (4.16) and (4.18):

$$\Omega_{gw}(k, \tau) = \frac{k^4}{12 \pi^2 H^2 \overline{M}_P^2 a^4} \left| \frac{c_{re}(k)}{c_{ex}(k)} \right|^2 \left(1 + \frac{1}{k^2 \tau_{re}^2} \right). \quad (4.23)$$

As already mentioned twice, in Eq. (4.23) we have two complementary possibilities depending on the nature of the turning point¹⁸. When the wavelength enters the Hubble radius during radiation the correct limit is $k\tau_{re} \ll 1$ and the spectral energy density at high-frequency can then be estimated as:

$$\Omega_{gw}(k, \tau_0) = \frac{k^2 n_*}{12 \pi^2 a_{ex}^2 \overline{M}_P^2} \left(\frac{H_{re}^2 a_{re}^4}{H_0^2 a_0^4} \right). \quad (4.24)$$

For the slice of wavenumbers $a_* H_* < k < a_1 H_1$ the exit takes place after the refractive phase where $a_{ex} = n_*^{-1/(1-\epsilon)} |k \tau_1|^{1/(1-\epsilon)}$. From Eq. (4.24) we then obtain:

$$h_0^2 \Omega_{gw}(\nu) = \left(\frac{H_1}{\overline{M}_P} \right)^2 \overline{\Omega}_* \left(\frac{\nu}{\nu_*} \right)^{m_T}, \quad \nu_* < \nu < \nu_{max}, \quad (4.25)$$

$$\overline{\Omega}_* = \frac{4 h_0^2 \Omega_{R0}}{3\pi} n_*^3 \left(1 + \frac{\alpha}{1 - \epsilon} \right)^{m_T} e^{-m_T \Delta N}, \quad (4.26)$$

where, as usual, $\Delta N = (N_t - N_*)$. The same reasoning for lower frequencies leads to:

$$h_0^2 \Omega_{gw}(\nu) = \left(\frac{H_1}{\overline{M}_P} \right)^2 \overline{\Omega}_* \left(\frac{\nu}{\nu_*} \right)^{n_T}, \quad \nu_{eq} < \nu < \nu_*, \quad (4.27)$$

$$h_0^2 \Omega_{gw}(\nu) = \left(\frac{H_1}{\overline{M}_P} \right)^2 \overline{\Omega}_* \left(\frac{\nu}{\nu_*} \right)^{n_T} \left(\frac{\nu}{\nu_{eq}} \right)^{-2}, \quad \nu < \nu_{eq}. \quad (4.28)$$

¹⁸If the reentry takes place during the radiation phase we have that, in the vicinity of $\tau_{re} a'' \rightarrow 0$ so that $k\tau_{re} \ll 1$ in Eq. (4.23). Conversely the modes exit during the inflationary phase when $\omega^2 \tau_{ex} \simeq 1$ (i.e. $k^2 \tau_{ex}^2 \simeq n_*^2$).

Equations (4.25)–(4.26) and (4.27)–(4.28) give $\Omega_{gw}(k, \tau)$ in the three spectral regions defined in Fig. 1. In summary the lowest frequency region involves the modes exiting the Hubble radius during the refractive phase and reentering after equality (i.e. $k < a_{eq}H_{eq}$). The intermediate region concerns the modes exiting the effective horizon during the refractive phase and reentering during radiation (i.e. $a_{eq}H_{eq} < k < a_*H_*$). The highest frequency domain encompasses the modes that exit the Hubble radius after the end of the refractive phase and reenter during radiation (i.e. $a_*H_* < k < a_1H_1$). As we shall see the relevant physical regime is the one where the rate of variation of n is larger than ϵ ; in this limit we can expand the spectral index for $\epsilon \ll 1$:

$$n_T = \frac{3\alpha - 2\epsilon}{(1 + \alpha - \epsilon)} = \frac{3\alpha}{1 + \alpha} + \frac{[-2 + \alpha(1 - 2\gamma)]\epsilon}{(1 + \alpha)^2} + \mathcal{O}(\epsilon^2), \quad (4.29)$$

where the second equality follows in the limit $\epsilon \ll 1$. The spectra obtained so far in the case of a dynamical refractive index are fully compatible with a conventional inflationary stage and this is ultimately the reason for the flatness of $\Omega_{gw}(k, \tau)$ at high-frequencies. It is however interesting to mention that the parametrization of Eqs. (4.25)–(4.26) and (4.27)–(4.28) holds also, with the appropriate differences, when the spectrum at intermediate frequencies is not dictated by the evolution of the refractive index. Two cases are particularly important in the light of the current data: the bounces of the scale factor and the curvature bounces. For a bounce of the scale factor the scale factor first contracts in an accelerated manner¹⁹ and then undergoes a stage of decelerated expansion (i.e. $\dot{a} > 0, \ddot{a} < 0$). In the case of an accelerated contraction the scale factor can be parametrized as a power-law $a(t) \simeq (-t/t_1)^\delta$ with $0 < \delta < 1$. When $\delta < 0$ we have instead an accelerated expansion with growing curvature (i.e. $\dot{H} > 0$). The spectral energy density of the relic gravitons produced in this kind of scenarios can be estimated as in the previous case with the relevant similarity that the intermediate spectral index is also blue. In the case of accelerated contraction we have

$$n_T = 3 - \left| \frac{2\delta}{\delta - 1} - 1 \right|, \quad 0 < \delta < 1. \quad (4.30)$$

In the case of accelerated expansion with $\delta < 0$ we have instead

$$n_T = \frac{2}{|\delta| + 1}, \quad \delta < 0. \quad (4.31)$$

For $\nu > \nu_*$ the slope s controlled by m_T even if, in this case, the quasi-flat slope is not related to a slow-roll dynamics as in the conventional inflationary case. We can therefore conclude that $\bar{\Omega}_*$ is generally given by the product of two separate contributions

$$\bar{\Omega}_* = \bar{\Omega}_{late}(\Omega_{R0}, \Omega_\Lambda, N_{eff}, N_\nu) \bar{\Omega}_{early} \quad (4.32)$$

where $\bar{\Omega}_{late}$ denotes the late-time contribution that only depends on the parameters of the concordance scenario; in Eq. (4.32) $\bar{\Omega}_{early}$ is instead the early contribution that is generally model-dependent. In particular we have that, in the present case, $\bar{\Omega}_* = \bar{\Omega}_*(\alpha, \epsilon, N_*, N_t)$.

¹⁹This means that $\dot{a} < 0$ and $\ddot{a} < 0$ where, only in this paragraph, the overdot denotes a derivation with respect to the cosmic time coordinate t .

4.4 High-frequency normalization of the spectral energy density

The high-frequency normalization can be studied accurately by considering all the late-time sources of suppression but this analysis is postponed to the following section since, in what follows, the attention is focused on the general logic that can be more directly appreciated from the analytic results deduced above. The first observation is that in the conventional situation (H_1/M_P) appearing in Eq. (4.25) is fixed from the amplitude of the scalar power spectrum $\mathcal{A}_{\mathcal{R}}$ and from the slow-roll parameter:

$$\left(\frac{H_1}{M_P}\right) = 4.7 \times 10^{-6} \left(\frac{\mathcal{A}_{\mathcal{R}}}{2.41 \times 10^{-9}}\right)^{1/2} \left(\frac{\epsilon}{0.003}\right)^{1/2}. \quad (4.33)$$

When the normalization is set at low-frequencies ϵ is related to the r_T whose upper limits fix the spectral energy density in the aHz range. In the present case, however, the situation is different and there are, in purely abstract terms, two complementary possibilities:

- the first logical possibility is to fix the normalization by requiring that the spectral energy density matches the value measured by the PTA at the typical frequency $\nu = \nu_P = \mathcal{O}(30)$ nHz;
- the second possibility is instead to normalize the potential signal in the audio band by enforcing the LVK bound at the frequency $\nu = \nu_L = \mathcal{O}(60)$ Hz.

Between these two possibilities the latter is more plausible than the former for the simple reason that, generally speaking, $\nu_* < \nu_L$ so that the quasi-flat branch of the spectrum falls in the audio band. On the other hand it is plausible to have that ν_* is either larger or smaller than ν_P . This point is illustrated in Fig. 2 where the darker area defines the region where $100 \text{ aHz} < \nu_* < \nu_P$. The various labels appearing on the curves define the common logarithm of ν_* expressed in Hz. We have that, approximately, $\nu_P = \mathcal{O}(10^{-7.5})$ Hz. Figure 2 explains why the high-frequency normalization has been fixed by requiring

$$\left(\frac{H_1}{M_P}\right)^2 \bar{\Omega}_* \left(\frac{\nu_L}{\nu_*}\right)^{m_T} = h_0^2 \bar{\Omega}_{gw}(\nu_L), \quad \nu > \nu_*. \quad (4.34)$$

According to Eqs. (3.2)–(3.3) the absolute upper limit for the quasi-flat spectral energy density should be $\mathcal{O}(5.8) \times 10^{-9}$ and, for the sake of simplicity, we are going to require, in a conservative perspective²⁰, that $\bar{\Omega}_{gw}(\nu_L) = 5.8 \times 10^{-9}$. To illustrate the procedure (and to avoid the possible complications that are addressed in the next section) we assume, in the notations of Eq. (4.32), that

$$\bar{\Omega}_{late}(\Omega_{R0}) = \frac{4}{3\pi} \Omega_{R0}, \quad (4.35)$$

$$\bar{\Omega}_{early}(\alpha, \epsilon, N_*, N_t) = e^{3\alpha N_*} \left(1 + \frac{\alpha}{1 - \epsilon}\right)^{m_T} e^{-m_T \Delta N}. \quad (4.36)$$

From Eqs. (4.34) and (4.35)–(4.36) the following relation can be deduced

$$e^{[3 - m_T(\epsilon)]\alpha N_*} e^{m_T(\epsilon)\Delta N} = \frac{3}{4} \left[\frac{\Omega_{gw}(\nu_L)}{\Omega_{R0} \epsilon \mathcal{A}_{\mathcal{R}}}\right] \left(\frac{\nu_{max}}{\nu_L}\right)^{m_T(\epsilon)}. \quad (4.37)$$

²⁰This estimate ignores, by explicit choice, the sources of damping that have been instead taken into account in section 5. It must be understood as an order of magnitude evaluation. In Fig. 4 the various later-time damping sources have been included and the obtained results are compared with the analytic estimates. In spite of the (obvious) slight numerical disagreement it turns out that the analytic results are quite useful to illustrate the general logic.

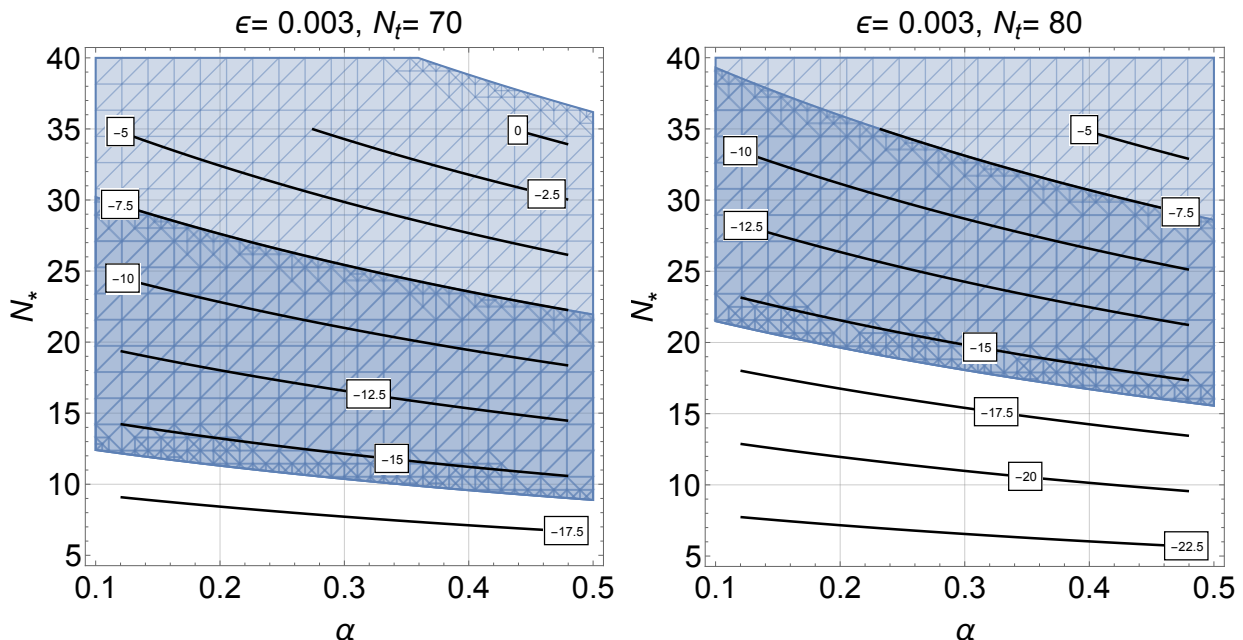


Figure 2: The shaded area illustrates the region of the parameter space where, according to Eq. (4.22), $100 \text{ aHz} < \nu_* < \nu_L$. The two plots differ because of the total number of e -folds but are otherwise qualitatively similar. The darker region in the central part of both plots corresponds to $100 \text{ aHz} \nu_* < \nu_P$. The various curves are the contours where the values of ν_* remain the same and in the labels we report the common logarithm of ν_* expressed in Hz.

As we mentioned in Eq. (3.2) the value of ν_L ranges approximately between 20 and 76 Hz. This range is related to the frequency region which is more sensitive to the backgrounds of relic gravitons; for the sake of concreteness we therefore posit $\nu_L = 60$ Hz. To pass from Eq. (4.37) we first employed Eq. (4.34) and also noted that $\nu_L/\nu_* = (\nu_L/\nu_{max})(\nu_{max}/\nu_*)$ since the ratio (ν_{max}/ν_*) can be directly estimated from Eq. (4.22). In practice all the terms at the left of Eq. (4.37) contain the parameters of the model while the quantities at the right-hand side are either directly measured or can be determined as late-time parameters of the concordance paradigm. For a swift estimate of the parameters the right-hand side of Eq. (4.37) can be evaluated in the limit $m_T(\epsilon) \ll 1$. If we now take the logarithm of both sides of Eq. (4.37) we obtain

$$[3 - m_T(\epsilon)] \alpha N_* + \Delta N m_T(\epsilon) = 15.62 + 15.31 m_T(\epsilon) \quad (4.38)$$

In the limit $m_T(\epsilon) \ll 1$ Eq. (4.38) roughly implies $3\alpha N_* \simeq 15.62$. This means that α and N_* are inversely proportional: a longer refractive phase imposes a smaller α and vice-versa. Having determined the normalization according to Eq. (4.38) we can directly write spectral energy density as

$$\begin{aligned} h_0^2 \Omega_{gw}(\nu) &= \mathcal{B}(\nu_L) \left(\frac{\nu}{\nu_*} \right)^{m_T(\epsilon)}, & \nu_* < \nu < \nu_{max}, \\ h_0^2 \Omega_{gw}(\nu) &= \mathcal{B}(\nu_L) \left(\frac{\nu}{\nu_*} \right)^{n_T(\alpha, \epsilon)}, & \nu_{eq} < \nu < \nu_*, \end{aligned}$$

$$h_0^2 \Omega_{gw}(\nu) = \mathcal{B}(\nu_L) \left(\frac{\nu}{\nu_*} \right)^{n_T(\alpha, \epsilon)} \left(\frac{\nu_{eq}}{\nu} \right)^2, \quad \nu < \nu_{eq}, \quad (4.39)$$

where we stress that $\mathcal{B}(\nu_L) = 10^{-8.61}$ has been fixed by normalising the spectral energy density to the largest value compatible with the LVK bound. Since we already saw from Fig. 2 that the values of ν_* can be either larger or smaller than ν_P it is natural to parametrize ν_* in terms of ν_P by setting $\nu_* = f_0 \nu_P$ where f_0 can be either smaller or larger than 1. The discussion developed so far assumes

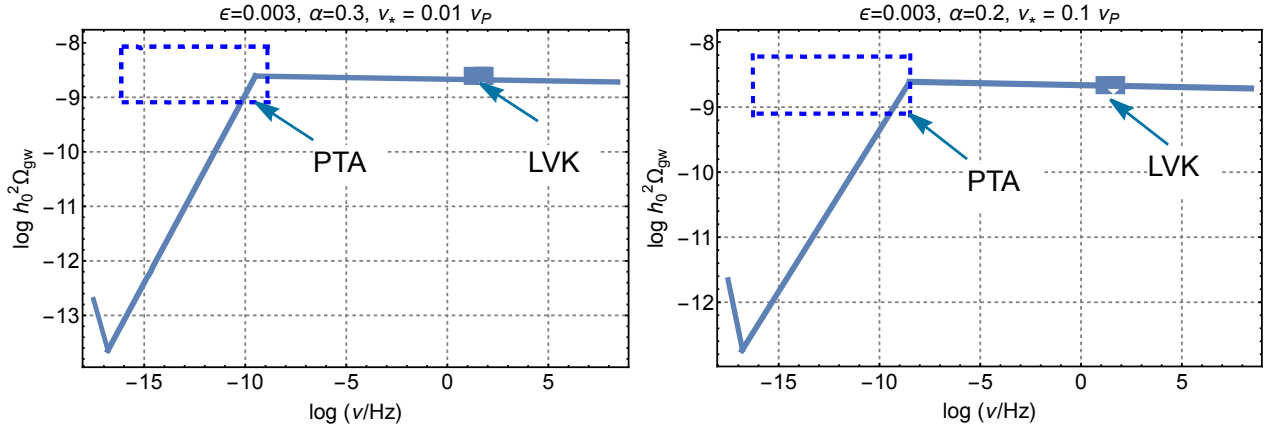


Figure 3: The analytic result of Eq. (4.38) is illustrated for different values of the parameters. The dashed region defines the purported PTA signal while the LVK limit is automatically taken into account by enforcing the high-frequency normalization. We note that these two plots refer to a pair of different values of ν_* that have been purposely selected around the reference frequency of the PTA which is of the order of 31.68 nHz (see Tab. 2 and Eq. (3.4)). Note that the region with the dashed perimeter corresponds to $q_0 = \bar{q}_0 = 2.467$ in Eqs. (3.6) and (3.8).

a conventional inflationary stage where H_1/M_P is determined from the scalar power spectrum and, in this case, Eq. (4.33) holds. The same strategy adopted above can however be applied also in the complementary situation where the universe bounces across a typical curvature scale of the order of H_1 . In this case the spectral energy density for $\nu > \nu_*$ is given by:

$$h_0^2 \Omega_{gw}(\nu) = \frac{4h_0^2 \Omega_{R0}}{3\pi} \left(\frac{H_1}{M_P} \right)^2 \quad \nu > \nu_*. \quad (4.40)$$

The main difference is that in the case of Eq. (4.40) the scale H_1 cannot be estimated as in Eq. (4.33). On the contrary it is exactly the LVK bound that sets the scale of H_1 :

$$\frac{H_1}{M_P} = 6.65 \times 10^{-3} \left(\frac{h_0^2 \Omega_{R0}}{4.15 \times 10^{-5}} \right)^{-1/2} \left(\frac{h_0^2 \Omega_{gw}(\nu_L)}{2.45 \times 10^{-9}} \right)^{1/2}. \quad (4.41)$$

As already mentioned the results of Eqs. (4.38) and (4.40)–(4.41) do not include the late-time damping that has the effect of shifting a bit the above estimates as we shall see in the following section. The logic of this section has been to deduce analytically the high-frequency plateau and to normalise its value to the LVK bound.

5 Phenomenological considerations

The previous section illustrates how the PTA data and the constraints provided by the LVK collaboration set the normalization of the spectral energy density without any reference to the low-frequency data of the aHz region. The general expression of the high-frequency amplitude consists of two contributions that are formally distinguished in Eq. (4.32). In the previous section, for the sake of simplicity, only the leading contribution to the late-time suppression has been included while some of the phenomena that may further suppress the high-frequency plateau have been neglected. Even though the considerations presented hereunder are relevant, from a quantitative viewpoint, for an improved determination of the theoretical template, the general logic pursued so far remains unaltered.

If the late-time contribution (i.e. $\bar{\Omega}_{late}$ in Eq. (4.32)) is reduced, the early-time contribution may become comparatively larger whenever the high-frequency normalization is imposed (see also Eqs. (4.35)–(4.36)). In this respect it is useful to answer three separate questions. The first one concerns the overall magnitude of the suppression in the high-frequency domain where the normalization is set. The second issue calls for a distinction between the damping effects that depend on the frequency and the ones that are instead frequency-independent. It is finally useful to gauge the relative error on the spectral energy density when these effects are simply neglected, as tentatively assumed in the previous section.

5.1 Impact of the neutrino free streaming

The effect of neutrino free streaming on the spectral energy density of the relic gravitons has been first pointed out by in Ref. [58] (see also [59, 60, 61, 62]) where the various authors first argued and then confirmed that the correction to the spectral energy density is mildly dependent on the frequency and it is overall of the order of the 10 %. Since the effect of neutrino free-streaming is fully operational for $\nu < \nu_{bbn}$ it is comparatively less relevant for the high-frequency normalization. The logic is that, after neutrino decoupling, the neutrinos free stream and the effective energy-momentum tensor acquires, to first-order in the amplitude of the plasma fluctuations, an anisotropic stress. In the present case the spectral energy density at intermediate frequencies is not quasi-flat (as in the standard case) but it increases as a function of the frequency but still the magnitude of the effect depends on R_ν , i.e. the neutrino fraction in the radiation plasma:

$$R_\nu = \frac{\rho_\nu}{\rho_\gamma + \rho_\nu} = \frac{3 \times (7/8) \times (4/11)^{4/3}}{1 + 3 \times (7/8) \times (4/11)^{4/3}} = 0.4052. \quad (5.1)$$

In Eq. (5.1) 3 counts the degrees of freedom associated with the massless neutrino families, $(7/8)$ arises because neutrinos follow the Fermi-Dirac statistics; the factor $(4/11)^{4/3}$ stems from the relative reduction of the neutrino (kinetic) temperature (in comparison with the photon temperature) after weak interactions fall out of thermal equilibrium. Assuming that the only collisionless species in the thermal history of the Universe are the neutrinos and recalling Eq. (5.1), the amount of suppression can be parametrized by the function

$$\mathcal{M}(R_\nu) = 1 - 0.539R_\nu + 0.134R_\nu^2. \quad (5.2)$$

This suppression is effective for relatively small frequencies which are larger than ν_{eq} and smaller than ν_{bbn} . In what follows we shall stick to the case of the Λ CDM paradigm [5, 6, 7] but more complicated examples do not change the nature of the effect.

5.2 Impact of the decoupling of relativistic species

The late-time suppression of the spectral energy density of Eqs. (4.32) and (4.35) has been estimated by simply positing that the late Universe is dominated by radiation down to the equality epoch. If the evolution of the relativistic species is neglected we have that $a^4 H^2$ is roughly constant during radiation. In practice to get an approximate expression of $\bar{\Omega}_{late}$ we need to evaluate

$$\frac{a_{re}^4 H_{re}^4}{a_0^4 H_0^2} = \left(\frac{a_{re}^4 H_{re}^4}{a_{eq}^4 H_{eq}^2} \right) \left(\frac{a_{eq}^4 H_{eq}^4}{a_0^4 H_0^2} \right). \quad (5.3)$$

In the context of the concordance paradigm, the first bracket at the right-hand side of Eq. (5.3) is evaluated during the radiation stage and it does not introduce any suppression as long as $a^4 H^2$ is strictly constant. This conclusion is, however, slightly inaccurate because of the evolution of the relativistic species. In local thermal equilibrium the total entropy and energy densities of a relativistic plasma can be written, respectively, as $s_t = 2\pi^2 g_s(T) T^3 / (45)$ and as $\rho_t = \pi^2 g_\rho(T) T^4 / (30)$ where T is the common temperature of all the species of the plasma. At the plasma cools down the effective number of spin degrees of freedom appearing in the total entropy density and in the total energy density (i.e. $g_\rho(T)$ and $g_s(T)$) eventually decrease in a computable manner depending on the microscopic description of the plasma. If all the species of the plasma are in local thermal equilibrium at the same temperature we have that g_s and g_ρ coincide and this is what happens in the standard model for temperatures larger than the top quark mass where $g_s = g_\rho = 106.75$. The evolution of the relativistic species suggests that, during the radiation stage,

$$\left(\frac{a_r^4 H_r^2}{a^4 H^2} \right) = \left(\frac{g_\rho(T_r)}{g_\rho(T)} \right) \left(\frac{g_s(T)}{g_s(T_r)} \right)^{4/3}. \quad (5.4)$$

In principle if a given mode k reenters the Hubble radius at a temperature T_k the spectral energy density of the relic gravitons is (kinematically) suppressed by a factor which can be estimated as $[g_\rho(T_k)/g_{\rho 0}][g_s(T_k)/g_{s 0}]^{-4/3}$ [63, 64, 65]; at the present time $g_{\rho 0} = 3.36$ and $g_{s 0} = 3.90$. In general terms the effect parametrized by Eq. (5.4) will cause a frequency-dependent suppression, i.e. a further modulation of the spectral energy density $\Omega_{gw}(k, \tau_0)$. The maximal suppression one can expect follows by inserting into Eq. (5.4) the largest g_s and g_ρ . So, in the case of the minimal standard model this would imply that the suppression (on $\Omega_{gw}(k, \tau_0)$) will be of the order of $\mathcal{O}(0.38)$. In popular supersymmetric extension of the minimal standard model g_ρ and g_s can be as large as $\mathcal{O}(230)$ reducing the previous estimate to $\mathcal{O}(0.29)$. These considerations demonstrate, a posteriori, the overall correctness of the assumptions behind Eq. (5.4) and its descendants.

5.3 Impact of the dominance of dark energy

The largest wavelengths of the spectrum crossed Hubble radius about 65 e -folds before the end of inflation and reentered when dark energy was already dominant. In the vanilla Λ CDM scenario the role of the dark energy is played by the cosmological constant and since the evolution of $|aH|$ is monotonically decreasing for $a_{eq} < a < a_\Lambda$, all the wavelengths that left the Hubble radius during inflation will remain within the Hubble radius after they reenter either during radiation or during matter dominance. If we also consider the evolution for $a > a_\Lambda$, the behaviour of $|aH|$ is, overall, non-monotonic: a bunch of wavelengths that reentered after equality will again exit after dark energy

dominates at the redshift

$$1 + z_\Lambda = \left(\frac{a_0}{a_\Lambda}\right) = \left(\frac{\Omega_\Lambda}{\Omega_{M0}}\right)^{1/3}. \quad (5.5)$$

We can now consider the mode $k_\Lambda = a_\Lambda H_\Lambda$, i.e. the mode approximately reentering the Hubble radius at τ_Λ . Since H is approximately constant for $a > a_\Lambda$ we have that $H_\Lambda \equiv H_0$ where H_0 is the present value of the Hubble rate. A typical wavenumber that is today of Hubble size (i.e. $k_0 = a_0 H_0$) is larger than k_Λ even if, according to a superficial intuition, it should be smaller²¹ and this is because of the non-monotonic evolution of aH . This range of wavelengths is currently inside the Hubble radius and their power spectrum is given by:

$$P_T(k, \tau_0) = P_T(k, \tau_{re}) \left(\frac{a_{re}}{a_\Lambda}\right)_{\text{mat}}^2 \left(\frac{a_\Lambda}{a_0}\right)_\Lambda^2 \equiv P_T(k, \tau_{re}) \left(\frac{k_\Lambda}{k}\right)^4 \left(\frac{\Omega_{M0}}{\Omega_\Lambda}\right)^{2/3}, \quad k_0 < k < k_{eq}. \quad (5.6)$$

The spectral energy density when the relevant wavelengths are inside the Hubble radius can be obtained from Eq. (5.6) and the result is:

$$\begin{aligned} \Omega_{gw}(k, \tau_0) &= \frac{P_T(k, \tau_{re})}{12} \left(\frac{k}{k_0}\right)^{-2} \left(\frac{k_\Lambda}{k_0}\right)^4 \left(\frac{\Omega_{M0}}{\Omega_\Lambda}\right)^{2/3} \\ &= \frac{P_T(k, \tau_{re})}{12} \left(\frac{k}{k_0}\right)^{-2} \left(\frac{\Omega_{M0}}{\Omega_\Lambda}\right)^2, \quad k_0 < k < k_{eq}, \end{aligned} \quad (5.7)$$

where we used that, by definition, $k_\Lambda/k_0 = (\Omega_{M0}/\Omega_\Lambda)^{1/3}$. If the dominance of dark energy is completely neglected, Eq. (5.7) can be written in the same form where, however, the term $(\Omega_{M0}/\Omega_\Lambda)^2$ is absent. We conclude that, in this branch of the spectrum, the dominance of dark energy suppresses the spectrum by a factor $(\Omega_{M0}/\Omega_\Lambda)^2 = (0.44)^2 = 0.193$.

The wavenumbers falling instead in the interval $k_\Lambda < k < k_0$ correspond to wavelengths reentering the Hubble radius during the matter-dominated epoch and exiting again the Hubble radius when dark energy is already dominant. These wavelengths are currently outside the Hubble radius. The same logic leading to Eq. (5.6) implies that the power spectrum in the interval $k_\Lambda < k < k_0$ is given by $P_T(k, \tau_{re}) (a_{re}/a_{ex})^2$ or, more precisely,

$$P_T(k, \tau_0) = P_T(k, \tau_{re}) \left(\frac{a_{re}}{a_\Lambda}\right)_{\text{mat}}^2 \left(\frac{a_\Lambda}{a_{ex}}\right)_\Lambda^2 \equiv P_T(k, \tau_{re}) \left(\frac{k_\Lambda}{k}\right)^6, \quad k_\Lambda < k < k_0. \quad (5.8)$$

Equation (5.8) gives the power spectrum for typical wavelengths that are larger than the Hubble radius at the present time. The wavelengths belonging to the interval $k_\Lambda < k < k_0$ reenter the Hubble radius but then exit again and while they are larger than the Hubble radius their power spectrum remains unchanged. This is why, in Eq. (5.8), the power spectrum is not suppressed by a further factor $(a_{re}/a_0)^2$: these wavelengths are larger than the Hubble radius at the present time and therefore the power spectrum remains constant exactly as in the case of the scales exiting the Hubble radius at the onset of inflation. Using the identity $k_\Lambda/k_0 = (\Omega_{M0}/\Omega_\Lambda)^{1/3}$ the spectrum of Eq. (5.8) can be written as:

$$P_T(k, \tau_0) = P_T(k, \tau_{re}) \left(\frac{k_0}{k}\right)^6 \left(\frac{\Omega_{M0}}{\Omega_\Lambda}\right)^2. \quad (5.9)$$

²¹The numerical difference between k_0 and k_Λ is rather insignificant since $k_\Lambda = (\Omega_{M0}/\Omega_\Lambda)^{1/3} k_0$ and $(\Omega_{M0}/\Omega_\Lambda)^{1/3} \simeq \mathcal{O}(0.7)$. For this reason k_0 , k_Λ and k_p are all coinciding within one order of magnitude. The wavenumbers falling in the interval $k_0 < k < k_{eq}$ correspond to wavelengths reentering the Hubble radius during the matter-dominated epoch and remaining inside the horizon later on.

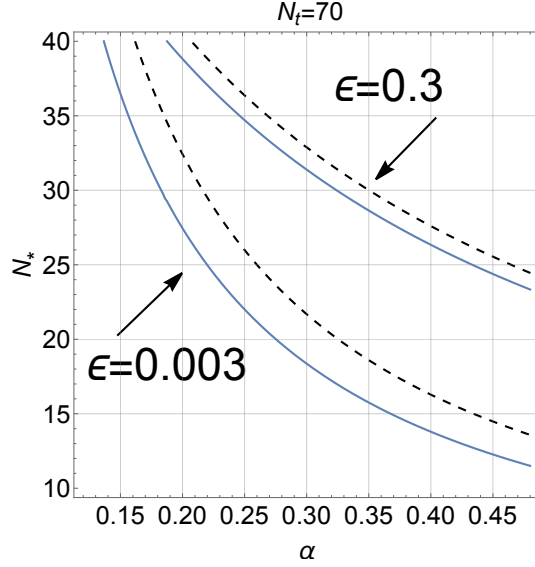


Figure 4: In the plane (α, N_*) we illustrate the normalization curve of Eq. (4.37). The dashed lines include the damping effects discussed in this section. The full line comes instead only from the estimates of the previous section. For the sake of illustration we selected $N_t = 70$ but different values for the total number of e -folds do not change the main features of the plot.

We can finally compute the spectral energy density in this interval and we obtain

$$\Omega_{gw}(k, \tau_0) = \frac{P_T(k, \tau_{re})}{12} \left(\frac{k}{k_0}\right)^{-4} \left(\frac{\Omega_{M0}}{\Omega_\Lambda}\right)^2, \quad k_\Lambda < k < k_0. \quad (5.10)$$

If the presence of dark energy would be neglected, $\Omega_{gw}(k, \tau_0)$ would scale as $(k/k_0)^{-2}$ and the suppression going as $(\Omega_{M0}/\Omega_\Lambda)^2$ would be totally absent. Note finally that when $k = k_\Lambda$ Eq. (5.9) implies that $\Omega_{gw}(k_\Lambda, \tau_0)$ is only suppressed as $(\Omega_{M0}/\Omega_\Lambda)^{4/3}$.

5.4 Numerical discussion of the spectral energy density

After having assessed the main sources of damping at high-frequency we now go back to Eqs. (4.35)–(4.36) and (4.37) with the purpose of improving the quantitative evaluation of the late-time suppression. Since the neutrino free-streaming is only effective at comparatively low-frequencies, at the right-hand side of Eq. (4.37) we should add a further contribution, namely

$$\ln \left[\frac{g_\rho(T)}{g_\rho(T_r)} \right] + \frac{4}{3} \ln \left[\frac{g_s(T_r)}{g_s(T)} \right] - 2 \ln \left(\frac{\Omega_{M0}}{\Omega_\Lambda} \right) = \mathcal{O}(3). \quad (5.11)$$

Equation (5.11) gives in fact the maximal suppression in the audio band so that, assuming $m_T(\epsilon) \ll 1$ the condition (4.37) gets modified as $3\alpha N_* \simeq 18.62$. For the same reason the determination of Eq. (4.41) gets is also affected and it is now

$$\frac{H_1}{M_P} = 1.15 \times 10^{-2} \left(\frac{h_0^2 \Omega_{R0}}{4.15 \times 10^{-5}} \right)^{-1/2} \left(\frac{h_0^2 \Omega_{gw}(\nu_L)}{2.45 \times 10^{-9}} \right)^{1/2}. \quad (5.12)$$

In Fig. 4 we illustrate the normalization curves deduced in Eq. (4.37). In particular, while the full lines refer to the case when the late-time damping is neglected, the dashed curves include instead the

different sources of damping previously analyzed in this section. The contribution associated with the neutrino free-streaming affects frequencies that are approximately smaller than ν_{bbn} and, for this reason, they are less relevant for the high-frequency normalization. At intermediate frequencies the spectral energy density is instead affected and this observation is relevant for the potential signal of the PTA. This aspect is illustrated in Fig. 5 where the spectral energy density has been reported

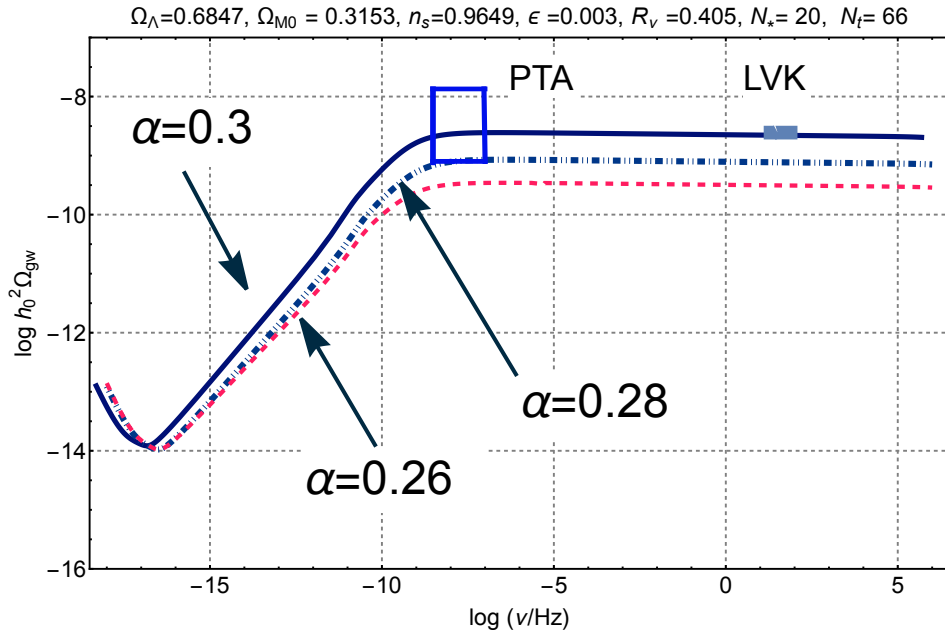


Figure 5: We illustrate the spectral energy density for different values of α . Common logarithm are employed on both axes. The effect of neutrino free-streaming is responsible for the suppression at intermediate frequencies. For the sake of illustration we consider $\alpha = \mathcal{O}(0.28)$ since $\alpha = 2/7$ ultimately corresponds to $\beta \rightarrow 2/3$ in Eqs. (3.4)–(3.5), and this is the value presumably suggested by the PTA determinations (see also Tab. 2). Note that the PTA region corresponds to $q_0 = \bar{q}_0 = 2.467$ in Eqs. (3.6) and (3.8).

for an illustrative choice of the parameters that is now specifically discussed. The pivotal parameters that determine the spectrum are primarily α , N_* and N_t . When N_* and N_t are of the same order the transition to normalcy occurs at the end of inflation but in this case it is impossible to get a large signal in the nHz range without jeopardizing the big-bang nucleosynthesis constraint of Eqs. (3.9)–(3.10). If we ought to address the PTA measurements we must require $N_* < N_t$ since, in this case, the transition to normalcy takes place before the onset of the radiation-dominated epoch (i.e. when the background is still inflating deep inside the quasi-de Sitter stage of expansion). In Fig. 5 we choose $N_t = 65$ and set $\epsilon = 0.003$. Even if this value has been deduced from the upper limits on r_T [5, 6, 7] and from the consistency we could easily consider values $\epsilon \ll 0.003$ and $r_T \ll 0.06$ since they are immaterial for the overall normalization but only for the slope $m_T(\epsilon)$ of the high-frequency plateau. The values of α appearing in Fig. 5 are around $\alpha \simeq 2/7$. In this case, the spectral index at intermediate frequencies is given by $n_T \simeq 2/3$, up to slow-roll corrections $\mathcal{O}(\epsilon)$ which are negligible since $\epsilon < 10^{-3}$. This value of α actually corresponds to $\beta = -2/3$ (see, in this respect, Tab. 2 and discussions thereafter). As discussed the PTA results are often reported in terms of a chirp amplitude

scaling as $\nu^{-2/3}$ for a typical reference frequency $\mathcal{O}(\text{yr}^{-1})$. The value $\alpha = 2/7 \simeq 0.28$ corresponds to $\beta = -2/3$ and $n_T \simeq 2/3$. More precisely we have that $\alpha = (2 + 4\epsilon)/7$ which can be approximated as $\alpha = 2/7 + \mathcal{O}(\epsilon)$ for $\epsilon < 10^{-3}$. In Fig. 5 the box illustrates the PTA measurements. In Fig. 5 the spectral energy density in critical units has been normalized by using the limits from the wide-band detectors given in Tab. 1 and by also imposing, as a particular choice, that $\alpha = \mathcal{O}(0.28)$ as suggested by the PTA measurements of Tab. 2. It is interesting that these two independent choices lead to a large signal in the nHz range when the variation of the refractive index occurs sufficiently early during the inflationary stage and anyway not beyond the first 20 e -folds. It is finally important to remark that, in the present context, then constraints on the integral of the spectral energy density of the relic gravitons (see Eqs. (3.9)–(3.10)) are automatically satisfied after imposing the normalization deduced from the direct limits set by the operating interferometers (see Tab. 1 and discussion thereafter).

6 Concluding remarks

Within the concordance paradigm the absolute normalization of the spectral energy density of the relic gravitons in critical units is assigned in the aHz region and it depends on r_T (i.e. the tensor to scalar ratio) that should not exceed $\mathcal{O}(0.06)$, at least according to the limits set by the temperature and polarization anisotropies of the microwave background. Since the Λ CDM is a compromise between the available data and the number of ascertainable parameters, the most stringent limits on r_T hold when the consistency relations between the scalar and tensor power spectra are enforced; in practice this only happens in the case of single-field inflationary models. If the spectral energy density of the cosmic gravitons is predominantly distributed for frequencies much larger than the aHz the logic leading to the low-frequency normalization is less compelling. In the nHz region the PTA recently reported a potential excess even if a bona fide signal coming from the relic gravitons should be correlated across the baselines and so far no indications along this direction have been obtained. Motivated by the improved limits in the audio band and by the current data from the pulsar timing arrays in the nHz domain, we analyzed the conditions for a quasi-flat spectrum of relic gravitons at intermediate and high-frequencies by introducing an improved physical strategy for the absolute normalization of the cosmic background of relic gravitons.

After proposing a general four-dimensional action for the discussion of relic gravitons in spatially flat backgrounds, we concentrated on the classes of scenarios where a large signal can be expected between the nHz and kHz ranges. While the most promising possibilities involve a dynamical refractive index and the bouncing dynamics, between these two cases the former is slightly more conservative than the latter insofar as it is compatible with the presence adiabatic and Gaussian initial data for the temperature and polarisation anisotropies of the microwave background. In both situations the spectral energy density increases over intermediate frequencies and then flattens out. Since the data from the wide-band detectors set the normalization of the spectral energy density at high-frequencies, a scheme based on the WKB method is preferable for a general estimate. Within this approach the early contributions can be easily distinguished from the late-time effects that are evaluated, depending on the convenience, in different approximations. The results obtained here also suggest an effective mechanism for the origin of a flat spectrum of relic gravitons with typical amplitudes that are even six or seven orders of magnitude larger than in the case of conventional inflationary models.

The results obtained here also suggest that the signal of the PTA can be explained by a background

of relic gravitons of inflationary origin without conflicting with the bounds coming from big-bang nucleosynthesis which are automatically satisfied as long as the data from wide-band interferometers set the normalization of the spectral energy density in critical units between few Hz and 0.1 kHz. In the present framework the low-frequency constraints can also be imposed a posteriori as a limit on the intermediate spectral slope but they are overall less crucial and they should be applied, strictly speaking, only when the consistency conditions between scalar and tensor modes are enforced.

Acknowledgements

The author is indebted to T. Basaglia, A. Gentil-Beccot, S. Rohr and J. Vigen of the CERN Scientific Information Service for their kind assistance.

References

- [1] L. P. Grishchuk, Sov. Phys. JETP **40**, 409 (1975) [Zh. Eksp. Teor. Fiz. **67**, 825 (1974)].
- [2] L. P. Grishchuk, Annals N. Y. Acad. Sci. **302**, 439 (1977).
- [3] L. H. Ford and L. Parker, Phys. Rev. D **16**, 1601 (1977).
- [4] A. A. Starobinsky, JETP Lett. **30**, 682 (1979) [Pisma Zh. Eksp. Teor. Fiz. **30**, 719 (1979)].
- [5] Y. Akrami *et al.* [Planck Collaboration], Astron. Astrophys. **641**, A10 (2020).
- [6] N. Aghanim *et al.* [Planck Collaboration], Astron. Astrophys. **641**, A6 (2020).
- [7] P. A. R. Ade *et al.* [BICEP and Keck], Phys. Rev. Lett. **127**, 151301 (2021).
- [8] V. A. Rubakov, M. V. Sazhin and A. V. Veryaskin, Phys. Lett. **115B**, 189 (1982).
- [9] R. Fabbri and M. D. Pollock, Phys. Lett. **125B**, 445 (1983).
- [10] L. F. Abbott and M. B. Wise, Nucl. Phys. **224**, 541 (1984).
- [11] S. Weinberg, *Cosmology*, (Oxford Univ. Press, Oxford UK, 2008).
- [12] M. Giovannini, Phys. Lett. B **668**, 44 (2008).
- [13] V. M. Kaspi, J. H. Taylor, and M. F. Ryba, Astrophys. J. **428**, 713 (1994).
- [14] F. A. Jenet *et al.*, Astrophys. J. **653**, 1571 (2006).
- [15] W. Zhao, Phys. Rev. D **83**, 104021 (2011).
- [16] P. B. Demorest *et al.*, Astrophys. J. **762**, 94 (2013).
- [17] W. Zhao, Y. Zhang, X. P. You and Z. H. Zhu, Phys. Rev. D **87**, 124012 (2013).
- [18] Z. Arzoumanian *et al.*, Astrophys. J. Lett. **905**, L34 (2020).
- [19] B. Goncharov *et al.* Astrophys. J. Lett. **917**, L19 (2021).
- [20] S. Chen, *et al.* Mon. Not. Roy. Astron. Soc. **508**, 4970 (2021).
- [21] J. Antoniadis *et al.*, [arXiv:2201.03980 [astro-ph.HE]].
- [22] M. Giovannini, Class. Quant. Grav. **33**, 125002 (2016).
- [23] M. Giovannini, Phys. Rev. D **98**, 103509 (2018).
- [24] B. Abbott *et al.* [LIGO Collaboration], Phys. Rev. D **69**, 122004 (2004).
- [25] B. Abbott *et al.* [LIGO Collaboration], Phys. Rev. Lett. **95**, 221101 (2005).
- [26] J. Abadie *et al.* [LIGO/Virgo Collaboration], Phys. Rev. D **85**, 122001 (2012).
- [27] J. Aasi *et al.* [LIGO/Virgo Collaboration], Phys. Rev. Lett. **113**, 231101 (2014).

- [28] J. Aasi *et al.* [LIGO/Virgo Collaboration], Phys. Rev. D **91**, 022003 (2015).
- [29] B. P. Abbott *et al.* [LIGO/Virgo Collaboration], Phys. Rev. Lett. **118**, 121101 (2017) Erratum: [Phys. Rev. Lett. **119**, 029901 (2017)].
- [30] B. P. Abbott *et al.* [LIGO/Virgo Collaboration], Phys. Rev. D **100**, 061101(R) (2019).
- [31] R. Abbott *et al.* [LIGO, Virgo and KAGRA collaborations], Phys. Rev. D **104**, 022004 (2021).
- [32] S. Weinberg, Phys. Rev. D **77**, 123541 (2008).
- [33] H. Motohashi and A. A. Starobinsky, JCAP **11**, 025 (2019).
- [34] M. Guerrero, D. Rubiera-Garcia and D. Saez-Chillon Gomez, Phys. Rev. D **102**, 123528 (2020).
- [35] A. Mohammadi, T. Golanbari, S. Nasri and K. Saaidi, Phys. Rev. D **101**, 123537 (2020).
- [36] M. Gasperini and M. Giovannini, Phys. Lett. B **287**, 56 (1992).
- [37] I. Antoniadis, J. Rizos and K. Tamvakis, Nucl. Phys. B **415**, 497 (1994).
- [38] Z. Guo and D. Schwarz, Phys. Rev. D **80**, 063523 (2009).
- [39] S. M. Carroll and E. A. Lim, Phys. Rev. D **70**, 123525 (2004).
- [40] W. Donnelly and T. Jacobson, Phys. Rev. D **82**, 081501 (2010).
- [41] J. D. Barrow, Phys. Rev. D **85**, 047503 (2012).
- [42] P. Szekeres, Annals Phys. **64**, 599 (1971).
- [43] P. C. Peters, Phys. Rev. D **9**, 2207 (1974).
- [44] M. Giovannini, Eur. Phys. J. C **82**, 117 (2022).
- [45] M. Giovannini, Phys. Rev. D **55**, 595 (1997).
- [46] M. Giovannini, Class. Quant. Grav. **22**, 2201 (2005).
- [47] S.-Y. Pi and R. Jackiw, Phys. Rev. D **68**, 104012 (2003).
- [48] M. Giovannini, Phys. Rev. D **99**, 083501 (2019).
- [49] N. Christensen, Phys. Rev. D **55**, 448 (1997).
- [50] B. Allen and J. Romano, Phys. Rev. D **59**, 102001 (1999).
- [51] D. Babusci and M. Giovannini, Phys. Rev. D **60**, 083511 (1999).
- [52] D. Babusci and M. Giovannini, Class. Quant. Grav. **17**, 2621 (2000).
- [53] M. Abramowitz and I.A. Stegun, *Handbook of Mathematical Functions* (Dover, New York, 1972).
- [54] A. Erdelyi, W. Magnus, F. Obehettinger, and F. Tricomi, *Higher Transcendental Functions* (McGraw-Hill, New York, 1953).

- [55] V. F. Schwartzmann, *JETP Lett.* **9**, 184 (1969).
- [56] M. Giovannini, H. Kurki-Suonio and E. Sihvola, *Phys. Rev. D* **66**, 043504 (2002).
- [57] R. H. Cyburt, B. D. Fields, K. A. Olive, and E. Skillman, *Astropart. Phys.* **23**, 313 (2005).
- [58] S. Weinberg, *Phys. Rev. D* **69**, 023503 (2004).
- [59] D. A. Dicus and W. W. Repko, *Phys. Rev. D* **72**, 088302 (2005).
- [60] H. X. Miao and Y. Zhang, *Phys. Rev. D* **75**, 104009 (2007).
- [61] K. W. Ng, *Phys. Rev. D* **86**, 103510 (2012).
- [62] B. A. Stefanek and W. W. Repko, *Phys. Rev. D* **88**, 083536 (2013).
- [63] Y. Watanabe and E. Komatsu, *Phys. Rev. D* **73**, 123515 (2006).
- [64] W. Zhao and Y. Zhang, *Phys. Rev. D* **74**, 043503 (2006).
- [65] K. Saikawa and S. Shirai, *JCAP* **1805**, 05, 035 (2018).